Studies on Circadian Clock RNA Methylation and Micturition Rhythm

(概日時計の RNA メチル化とミクチュリション日内変動の研究)

2020

伊藤　翔

Contents

Abstract

The circadian clock is composed of clock genes interlocked in transcriptional/post-translational feedback loops (TTFLs) regulating their own expression. The 2017 Nobel Prize in Physiology of Medicine was awarded for the works on the basic molecular mechanisms underlying TTFLs since 1984. In the decades since this discovery, most research on TTFLs has focused primally on two spatially and temporally separated processes: “transcription” and “(post)translation”. Yet, how these two processes are connected via RNA level regulation is poorly understood. Our laboratory found that RNA methylation is necessary for the proper function of the circadian clock: when RNA methylation is inhibited, the period of the circadian clock becomes longer. However, the molecular mechanisms underlying this phenomenon is not fully elucidated.

At the physiological level, the oscillations of the core clock genes in the TTFLs drive ~24h cycles in locomotor activity, body temperature and metabolism. Historically, recording methods of locomotor activity and body temperature rhythms have led to great advances in the study of circadian physiology. In addition, the development of the metabolic cage made it possible to measure food intake and energy consumption rhythms. However, methods for recording renal excretion and reabsorption rhythms are not well established and new methods with high accuracy are awaiting development.

In Chapter 1, the relationship between the circadian clock and RNA methylation

was investigated at the molecular level. Particularly, I focused on studying N^6-methyladenosine (m^6A), known as the most prevalent internal base modification of mRNA in mammals. I found that the transcripts of a key circadian clock component, Casein kinase 1 delta (*Csnk1d*), possess an m^6A modification in its 3′-untranslated region (3′-UTR). Reduced expression of the m^6A writer enzyme METTL3 led to the upregulation of CSNK1D protein expression, suggesting that the m^6A modification negatively regulates *Csnk1d* translation. To test the importance of m^6A of *Csnk1d in vivo*, I generated mutant mice with a deletion in the m^6A locus of the *Csnk1d* mRNA. The measurement of the locomotor activity of these mice demonstrated that the m^6A locus is required for the proper oscillations of the circadian clock. Furthermore, I showed that two uncharacterized CSNK1D isoforms generated via alternative splicing of the primary transcript, CSNK1D1 and CSNK1D2, exhibit mutually antagonistic functions in the regulation of the circadian clock.

In Chapter 2, I sought to optimize the “automated Voided Stain on Paper” (aVSOP), a system for measuring the circadian rhythms of renal excretion and reabsorption. The new improved method allows simultaneous measurement of rhythms in locomotor activity and micturition in freely moving mice, which was not possible before. To demonstrate the validity and accuracy of this improved system, I monitored simultaneously the locomotor and micturition rhythms under experimental jet-lag conditions, where the circadian clock function is temporarily impaired.

Chapter 1

RNA methylation controls the speed of the circadian clock via expression regulation of *Csnk1d*

Introduction

The regulation of gene expression at multiple levels allows cells that share a single genomic information to have a variety of phenotypes. In eukaryotes, the spatiotemporal separation of transcription and translation allows more complex gene expression regulation at the mRNA level. One example of such regulation is splicing, which contributed to the dramatic expansion of the protein-coding capacity of genes and facilitated the divergence of organisms [1]. Previous works to elucidate various regulations at the RNA level have advanced our understanding of cell biology, but little is known about the biological significance of RNA modifications.

To date, more than a hundred structurally distinct modifications have been identified in eukaryotic RNAs [2, 3]. Among these, N^6-methyladenosine (m^6A) is the most prevalent internal base modification in messenger RNA and long non-coding RNA in higher eukaryotes [4]. This modification is not static in cells, but dynamically written, read, and erased by specific proteins [5-7]. Recent studies demonstrated that m^6A is involved in the regulation of diverse physiological processes, such as heat shock response, fate determination of stem cells, X chromosome inactivation, and phase separation [8-10]. Our laboratory found that mRNA methylation is necessary for the proper function of the circadian clock: when mRNA methylation is inhibited, the period length of the circadian clock becomes longer [11]. However, the molecular mechanism underlying this phenomenon has not been fully elucidated.

The circadian clock is composed of clock genes interlocked in transcriptional/post-translational feedback loops (TTFLs) regulating their own expression [12, 13]. The *Per2* gene plays a central role in TTFL, and disruptions in *Per2* expression and function affect the entire clock system [14-16]. The stability and function of the PER2 protein is regulated by casein kinase 1 delta (CSNK1D, **Fig. 1**). CSNK1D is an essential serine/threonine protein kinase involved in various biological processes, such as meiosis, apoptosis, and ribosome assembly as well as circadian clock regulation [17-20]. Pharmacological inhibition, knockout, and RNA interference-mediated knockdown of CSNK1D are all known to elongate period length of the circadian clock, presumably due to the stabilization of the PER proteins [20-22].

In this Chapter, I found that *Csnk1d* transcripts possess m^6A in the 3′-untranslated region (3′-UTR), and demonstrated the physiological importance of m^6A-dependent regulation of *Csnk1d* expression. Furthermore, I showed that two uncharacterized *Csnk1d* isoforms generated via alternative splicing, CSNK1D1 and CSNK1D2, exhibit mutually antagonistic functions in the regulation of the circadian clock.

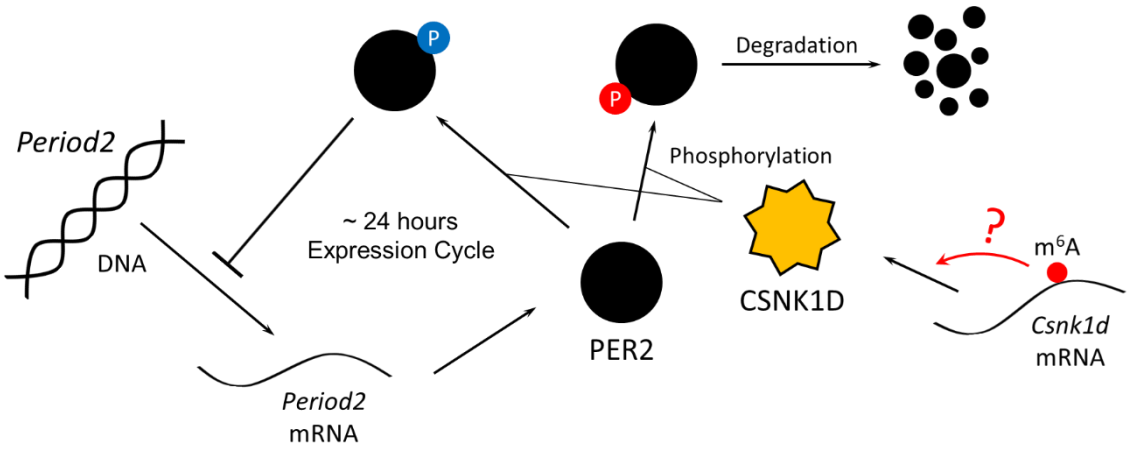

Fig. 1. Transcription-translation feedback loop and CSNK1D.

CSNK1D is known as a key clock regulator that phosphorylates the core clock component PER2. It is unknown how m^{6}A affects the expression of CSNK1D.

Materials and Methods

Animals

All experiments were approved by the animal experimentation committee of Kyoto University. 12 weeks old C57/BL6 males were maintained at 23 °C ± 1 °C with 50% ± 10% relative humidity, on a 12 h light / 12 h dark cycle (lights on 8:00, lights off 20:00), food and water ad libitum.

Deazaneplanocin A (DZ) brain infusion

Mice were transferred to respective cages under constant darkness for 9 to 11 days. The infusion cannula (Alzet, Brain Infusion Kit 2) connected with the osmotic pump (Altzet, pump model 1002) was directed stereotaxically to the SCN by surgery under anesthesia. The osmotic pump was implanted subcutaneously (dorsal skin) and continuously delivered 100 μM DZ to the SCN. After surgery, mice were returned to their home cages for 8 to 10 days.

Immunoblotting

Direct cell lysis using 2x Laemmli buffer supplemented with complete protease inhibitor +EDTA (Roche) and Phostop (Roche) followed by 10 min boiling at 95°C was used in all experiments. Proteins were separated on SDS-polyacrylamide gel, blotted onto PVDF membrane and detected with primary antibodies against CSNK1D

(Proteintech 14388-1-AP, 750x), METTL3 (Proteintech 15073-1-AP, 750x), ACTB (Sigma A5441, 1000x), and RPLP0 (aka RPLP0, Proteintech 11290-2-AP). CSNK1D quantification was performed using MultiGauge (FUJIFILM) and normalized by RPLP0 relative expression.

Quantitative RT-PCR

RNA was extracted using RNeasy Mini or Micro kit (Qiagen). Reverse transcription was performed with SuperScript VILO cDNA Synthesis kit (Thermo Fisher Scientific). Quantitative RT-PCR was performed using THUNDERBIRD SYBR Mix (TOYOBO) in StepOnePlus (Applied Biosystems). Data were normalized using relative expression of the housekeeping gene *Actb* or *Rplp0*.

Stable transfection of *Csnk1d* expression vectors

The coding sequence of *Csnk1d* isoforms were cloned into pSELECT-HYGRO-MCS vectors (Invivogen) with the primers 5′-TATGGATCCCAGTAGCGAGCCGCAC CGCTGCC-3′ and 5′-TATGCTAGCTCATCGGTGCACGACAGACTGAAG-3′, respectively containing overhanging *Bam*HI and *Nhe*I restriction sites for cloning. Vectors were then transfected into PER2::LUC MEFs with lipofectamine LTX (Invitrogen). 24h after transfection, cells were split into multiple replicate dishes and hygromycin was added to the medium. Medium was changed every three days, with hygromycin, until visible colonies formed. Single colonies were isolated with

conventional cloning cylinders then amplified. Monoclonal cell lines were first screened by Western Blot to ensure expression of the appropriate *Csnk1d* isoform.

siRNA mediated gene silencing

Silencing was performed with Stealth siRNA from Invitrogen. MEFs plated in 24-well plates at 70,000 cells/ml were transfected the next day with 40-80 pmol siRNA using 3 µl/well Lipofectamine 3000 (Invitrogen). For protein analysis by Western Blot shown on Fig. 1b, cells were sampled 48h later. For PER2::LUC cells and real-time luminescence shown in Fig. 5a, cells were plated at 70,000 cells/ml in 35 mm dishes, transfected the next day with 320 pmol siRNA and 16 µl Lipofectamine 3000. Sixteen hours later, medium was changed (antibiotics omitted), and 8 hours later cells were synchronized by a dexamethasone shock as described above.

Real-time luminescence measurements

Cells were seeded on 35-mm dishes and allowed to grow to confluence. Cells were then shocked by 200 nM dexamethasone for 2 h, followed by medium change containing 1 mM luciferin. Cells were then transferred to an 8-dishes luminometer-incubator (Kronos Dio, Atto). Photons were counted in bins of 2 min (Kronos Dio) at a frequency of 20 mins.

Liver mRNA preparation and Me-RIP

For each sample, about 200 mg liver piece from one mouse was collected in 4 ml RNeasy Midi RLT buffer (Qiagen) supplemented with β-mercaptoethanol, immediately homogenized and processed following manufacturer's instructions. mRNA was then purified from total RNA using Poly(A) mRNA Magnetic Isolation Module (NEBNext) scaled up to accommodate 50 µg total RNA, followed by an additional purification step using RNeasy MinElute columns (Qiagen). The obtained mRNA was further fragmented using Magnesium RNA Fragmentation Module (NEBNext), also followed by an additional purification step using RNeasy MinElute columns. Methylated mRNA fragments were then immunoprecipitated using protein A agarose beads (Roche) coupled to anti-m6A antibody (SYSY). 50 µl beads were incubated with 10 µg antibody in 0.1M PBS, T-X100 0.01%, 0.1 mg/ml BSA (IP buffer) for 2 h at 4 °C in a rotator. Beads-Ab were then washed 3 times with 1 ml IP buffer, then resuspended in 1 ml IP buffer with 5 µg 40-mer poly(A), and incubated for 1 h at 4 °C for pre-blocking. Beads-Ab were washed once with 1 ml IP buffer, then resuspended in 400 µl IP buffer. 5 µl RNasin PLUS (Promega) were added to the beads-Ab, followed by 2 µg fragmented mRNA; the mix was incubated 2 h at 4 °C in a rotator. Beads were then washed 3 times with 0.4 ml IP buffer with RNasin PLUS at 4 °C, then 2 times at RT. The final beads pellet was resuspended in 700 µl RLT buffer from MinElute kit, vortexed at full speed 10 sec 5 times and centrifuged at 1000 xg. The supernatant containing methylated mRNA fragments was transferred to a new tube and processed according

to MinElute protocol. cDNA library was synthesized as previously described [11].

Peak Calling was performed for each sample by MACS2 using sorted bam files. IntersectBed was used to determine peaks detected in 1 or 2 time points. To visualize peaks, MACS2 bdgcmp was performed on the treatment (me-RIP)- and control (input)-bedgraph outputs from MACS2 to deduct noise from me-RIP samples. These analyses were performed on the Galaxy server.

Polyribosome fractionation

24 hours before sampling, sucrose gradient was built by successively underlaying 2.2 ml of 10%, 20%, 30%, 40% and 50% sucrose solutions (Tris-HCl pH 7.5 20mM, MgCl2 10mM and KCl 100mM, 2mM DTT, murine RNase Inhibitor NEB 5ul/1000ul and cycloheximide 100 µg/ml) in 12 ml ultracentrifuge tubes (Beckman, 344059) using a Pasteur pipette mounted on a SOCOREX macropipette. Gradients were left for at least 24h at 4°C. The next day, ~80% confluent cells in 15 cm dishes were washed twice with ice-cold PBS, then incubated for 5 min in ice-cold PBS containing 100 µg/ml cycloheximide. PBS was decanted and cells were harvested on ice and transferred to a cold 2 ml microtube. Cells were centrifuged at 500xg for 5 minutes at 4°C. Supernatant PBS was discarded and cells were lysed in 6x of cell weight lysis buffer (20 mM Tris-HCl pH 7.5, 10 mM MgCl2, 100 mM KCl, 1% NP40, supplemented with EDTA-free cOmplete Protease Inhibitors (Roche), 2mM DTT, murine RNase Inhibitor (NEB, 1µl/40ul) and cycloheximide (100 µg/ml) for 10 min on ice after being passed 5

times through a 25G needle. The lysates were centrifuged 1300xg for 10 min at 4°C and the cleared lysates were transferred into new cold 1.5 ml tubes and kept on ice. 250 µl of cleared cell lysate as then carefully added on top of the sucrose gradient, one gradient for each lysate sample, and gradient were centrifuged at 36,000 RPM (Beckman Optima L ultracentrifuge, SW41 Ti rotor) at 4°C for 2 hours, with lowest acceleration and no brake. After centrifugation, each gradient was then split into 21 fractions by collecting 500 µl 6 aliquots from the top of the gradient, all steps performed at 4°C. Each fraction was mixed with 1500 µl Trizol LS (Invitrogen). RNA from each fraction was extracted following manufacturer's protocol and resuspended in the same volume of RNase-free water (50ul/fraction). Same volumes of RNA were then used for cDNA synthesis (VILO cDNA synthesis kit, Invitrogen). Transcript abundance in each fraction was quantified by quantitative real-time PCR with SYBR Green PCR Master Mix (Invitrogen), using the ΔCT method. The first (top most in the gradient) fraction was discarded from the data, as it contained no detectable mRNA, and the next fraction from the top of the gradient was used as a reference and set to 1 in each gradient data series.

Behavioral activity monitoring

Locomotor activity was measured with passive (pyroelectric) infrared sensors (FA-05 F5B, Omron) and the data were analyzed with ClockLab software (Actimetrics) developed on MatLab (Mathworks). Free-running circadian periods before or after surgery for DZ brain infusion were calculated from onset fitting. For mice with a −43-base pair (bp) deletion in the 3′-UTR of *Csnk1d*, free-running period was quantified by χ2 periodogram over the entire recording in constant darkness.

Primer and siRNA sequences

Quantitative real-time primer sequences were:

for *Csnk1d2*

5′-CTGCTCGTCTCCATCGGAAG-3′ and 5′-TTGGTAACAGAGTAGATCAGCC-3′,

for *Csnk1d1*

5′-CATGTCCACCTCACAGATTCC-3′ and 5’-TTGGTAACAGAGTAGATCAGCC-3,

for *Csnk1e*

5′-GAGACATCTACCTGGGTGCCA-3′ and 5′-ACCACTTGATGGACGGGATC-3′,

for *Rplp0*

5′-CTCACTGAGATTCGGGATATG-3′ and 5′-CTCCCACCTTGTCTCCAGTC-3′,

for *Mettl3*,

5′-TGATCTGGAGATAGAAAGCC-3′ and 5′-CAACAATGGACTGTTCCTTG-3′.

RNAi was performed with Stealth siRNA from Invitrogen:

custom 5′-GGGATATTCACATGGAGCTACCGTA-3’ for *Mettl3*;

custom 5′-GCATTCCTTTCGAACACCACGGCAA-3’ for *Csnk1d2*;

for *Per2*, PER2MSS207536, (MSS207537, MSS207538 gave similar results);

for pan*Csnk1d*, CSNK1DHSS102382, (CSNK1DHSS102383, CSNK1DHSS175379 worked equally).

1. 1 Regulation of CSNK1D expression by m^{6}A modification

Results

Csnk1d transcripts undergo m^{6}A modification in 3′-UTR

To identify clock-related transcripts regulated by m^{6}A, I quantified the m^{6}A levels in mouse liver mRNA. Fragmented mRNA was used as input for RNA immunoprecipitation with anti-m^{6}A antibodies, followed by RNA-seq (Me-RIP-seq, **Fig. 2a**). Several transcripts involved in the regulation of the circadian clock showed significant peaks. Among these, the most significant peak, according to the q value of the MACS2 peak-calling analysis, was the single peak in the 3′-UTR of the *Csnk1d* transcript (**Fig. 2b**), suggesting the possibility that CSNK1D expression is regulated by m^{6}A modification.

Methylation inhibitor deazaneplanocin A (DZ) induces CSNK1D

All trans-methylations, to various degrees, are influenced by the metabolic state of the cell due to their sensitivity to the availability of *S*-adenosylmethionine (SAM), the universal methyl donor co-substrate, and to the relative amount of the its by-product, *S*-adenosylhomocysteine (SAH), that acts as a competitive inhibitor [11]. Our

laboratory previously reported that 3-deazaadenosine (DAA), the most potent and frequently used inhibitor for SAH hydrolysis, can inhibit RNA methylation and cause circadian period elongation [11]. However, the nucleoside DAA also inhibits nucleotide synthesis and transcription. To pharmacologically inhibit RNA methylation and see its effect on *Csnk1d* expression without directly affecting transcription, I decided to use deazaneplanocin A (DZ), a carbocyclic analogue of DAA, that inhibits SAH hydrolysis without being metabolized as a nucleotide (**Fig. 3**).

The rhythmic locomotor activity of mammals is controlled by the master circadian clock that resides in the hypothalamic suprachiasmatic nucleus (SCN). First, to determine whether DZ affects master mammalian circadian clock in the same way as DAA, I continuously injected DZ into the third ventricle, just above the SCN, of freely moving mice (**Fig. 4a**). Mice exhibited a significant elongation of the activity rhythm period during DZ infusion compared to saline infused controls (CTL, 23.86 ± 0.06 h; DZ, 25.24 ± 0.09 h; $p<0.01$ in Bonferroni post hoc test after significant two-way ANOVA; **Fig. 4b**), which is approximately the same degree as the DAA shown in the previous report (CTL, 23.80 ± 0.08 hr; DAA, 24.88 ± 0.45 h, $p<0.01$ in Bonferroni post hoc test after significant two-way ANOVA) [11].

Next, to see the effect of DZ on CSNK1D expression, mouse embryonic fibroblasts (MEFs) were treated with DZ and then the expression of the CSNK1D protein was confirmed by immunoblotting. The CSNK1D proteins increased after 2 hours DZ treatment (**Fig. 4c, top**). This result is actually unexpected because previous studies

reported that (1) a decrease in CSNK1D causes period length elongation, and that (2) overexpression of CSNK1D causes period shortening [20, 23]. The reason why an increase in CSNK1D was accompanied by period elongation of the circadian clock will be investigated in the later of this chapter.

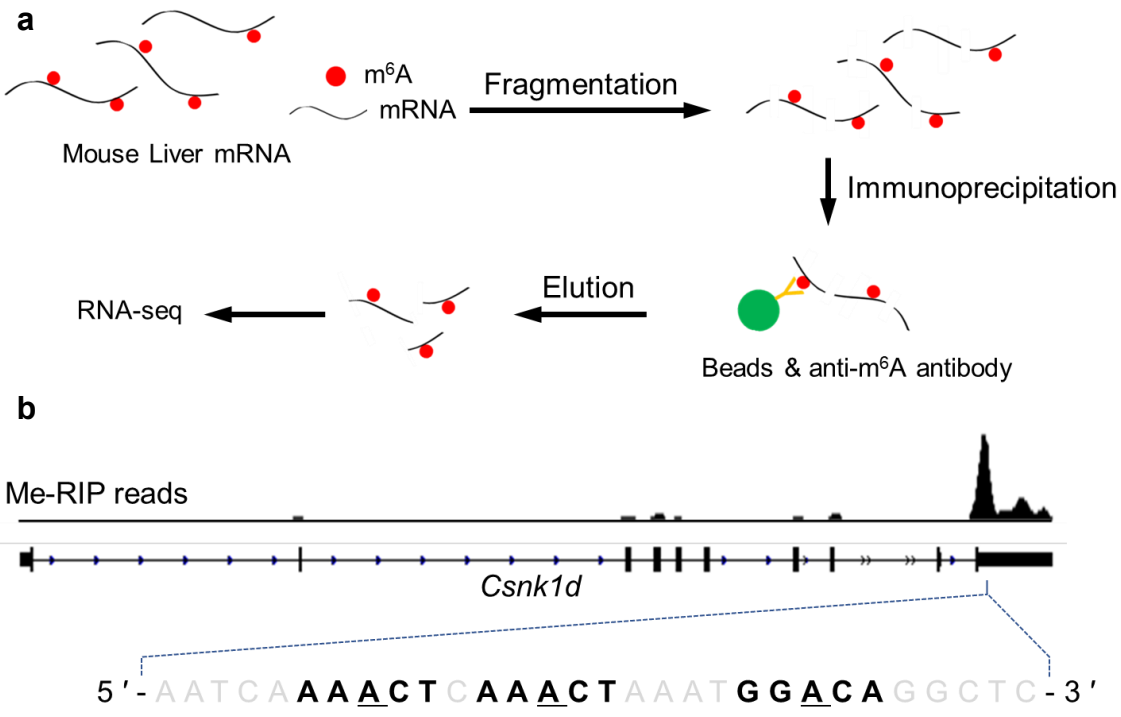

Fig. 2. Me-RIP seq revealed a *Csnk1d* m^{6}A peak

(a) Flow chart of Me-RIP seq. (b) MACS2 peak calling analysis revealed *Csnk1d* has a sharp, significant m^{6}A peak in 3′-UTR.

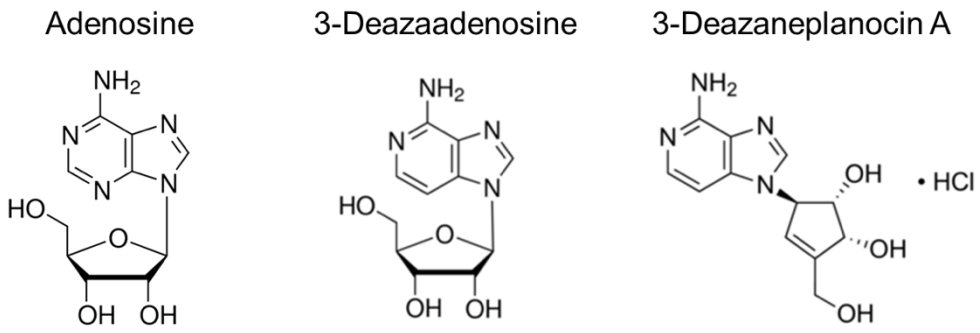

Fig. 3. Structures of adenosine, 3-deazaadenosine (DAA) and 3-deazaneplanocin A (DZ)

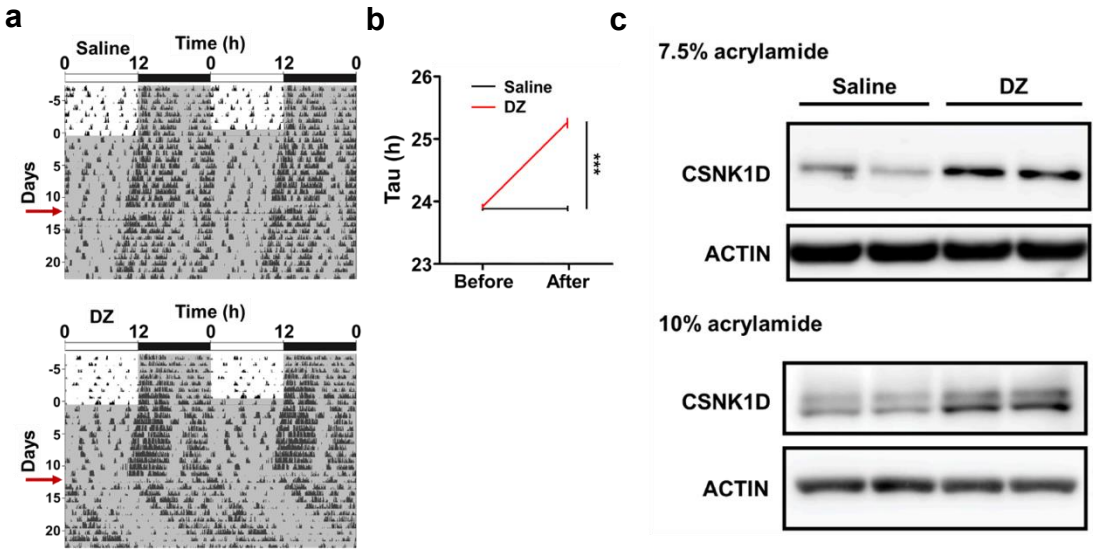

Fig. 4. DZ brain infusion and CSNK1D induction

(a) Locomotor activity of mice treated with DZ or Saline by brain infusion method. Surgery was performed on the day pointed by red arrow. White and gray background indicates lights on and off, respectively. (b) Brain DZ infusion (mice operated on the day indicated by brown triangles) increases the locomotor activity rhythm period. Graph on the bottom: mean ± SEM, analyzed in two-way ANOVA/Bonferroni analysis of n=9 CTL mice and n=6 DZ infused mice, with ***p<0.001. (c) 50-µM DZ treatment for 2 h increased CSNK1D protein level in mouse embryonic fibroblasts (MEFs). Two CSNK1D isoforms were observed when the total proteins from MEFs were run on a 10% SDS-polyacrylamide gel. ACTIN was used as a loading control.

Two alternative splicing isoforms of CSNK1D, CSNK1D1 and CSNK1D2

While repeating the experiments, I noticed the presence of two CSNK1D immunoreactive bands when the total proteins were electrophoresed on a 10% SDS-polyacrylamide gel, with the lower band being strongly induced by the DZ treatment (**Fig 4c, bottom**). In the database of National Center for Biotechnology Information, I found that there are two *Csnk1d* isoforms generated via alternative splicing; *Csnk1d1* (Human: NM_001893.6, Mouse: NM_139059.2) and *Csnk1d2* (Human: NM_139062.4, Mouse: NM_027874.2). Despite many reports on *Csnk1d*, there have been no studies focusing on the differences between the two alternative splicing isoforms in the control of circadian rhythms.

The *Csnk1d2* mRNA possesses a well conserved exon (Exon 9) that is skipped in the *Csnk1d1* mRNA, and inclusion/skipping of this exon causes C-terminal difference of the translated products (**Figs. 5a and b**). The *Csnk1d2* mRNA is longer than *Csnk1d1*, but the CSNK1D2 protein is shorter than CSNK1D1 because a stop codon is located in Exon 9. Since shorter proteins migrate faster than longer proteins in SDS-polyacrylamide gel electrophoresis, the lower band (shown in **Fig. 4c, bottom**) is presumed to represent the CSNK1D2 protein.

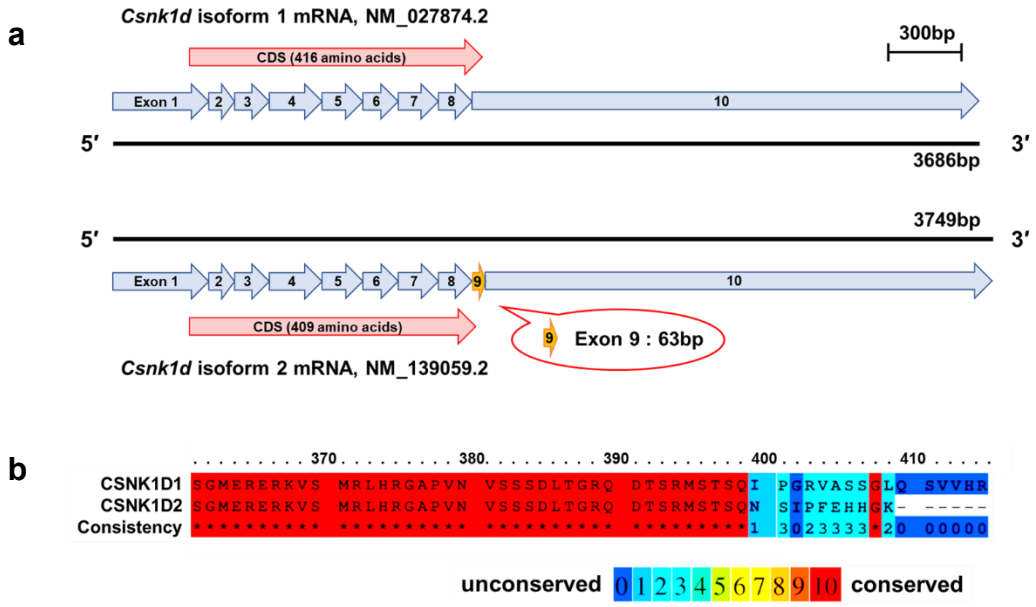

Fig. 5. Difference between two CSNK1D isoforms

(a) Alternative splicing of *Csnk1d* isoforms. (b) C-terminal difference between two CSNK1D isoforms. The mRNA for isoform 2 is longer than that of isoform 1, but encodes a shorter protein because of an in-frame stop codon in Exon 9.

DZ treatment induces *Csnk1d* isoforms at mRNA level.

To examine the effect of DZ on the mRNA expression levels of *Csnk1d* isoforms, I designed isoform-specific primer sets for quantitative RT-PCR (**Fig. 6a**). Melting curve analysis of PCR products amplified with these primer sets shows a single peak respectively, indicating successful target-specific amplification (**Fig. 6b**). Quantification of *Csnk1d* mRNA expression in DZ-treated MEFs revealed that *Csnk1d1* expression exhibited a modest increase, while *Csnk1d2* expression was markedly increased (**Fig. 6c**).

Next, to investigate how *Csnk1d* mRNA induction is triggered by DZ treatment, I measured the stability of *Csnk1d* transcripts under DZ treatment using Actinomycin D, a *de novo* transcription inhibitor (**Fig. 6d**). Although no significant stabilization by DZ was observed for both *Csnk1d* isoforms, I found the half-life of *Csnk1d1* was much shorter than *Csnk1d2*. This dramatic difference in mRNA stability is interesting because the *Csnk1d* isoforms differ by only one small exon (**Fig. 5a**). This result suggests that the small exon (Exon 9) plays an important functional role, directing these two isoforms to different subcellular contexts.

METTL3 silencing causes CSNK1D induction *in vitro*.

To confirm that the above results were dependent on mRNA m^6A inhibition, the

catalytic subunit of mRNA m^{6}A methyltransferase, METTL3 [5], was silenced in MEFs, and the protein levels of the CSNK1D isoforms were measured by immunoblotting. Silencing of METTL3 increased the intensity of both bands, presumably corresponding to CSNK1D1 and CSNK1D2, demonstrating that m^{6}A negatively regulates CSNK1D expression (**Fig. 7a**). Although this result was in good agreement with the result obtained by the DZ treatment (**Fig. 4c**), METTL3 silencing had no apparent effect on the mRNA levels of either of the CSNK1D isoforms (**Fig. 7b**), indicating that the regulation of CSNK1D expression by m^{6}A is not exactly the same as that by DZ.

Since the increase in the CSNK1D proteins under METTL3-silencing conditions cannot be readily explained by the amount of transcripts, I measured the effect of METTL3 silencing on translation by polysome fractionation (**Figs. 7c and 7d**). As a control, the expression of *Csnk1e*, which has no significant m^{6}A peak in Me-RIP-seq data, was also quantified. METTL3 silencing significantly increased *Csnk1d* transcript levels only in fractions containing heavier polysomes, while the level of the *Csnk1e* transcript was not significantly affected. These results suggest that the expression of CSNK1D is regulated by m^{6}A at the translational level.

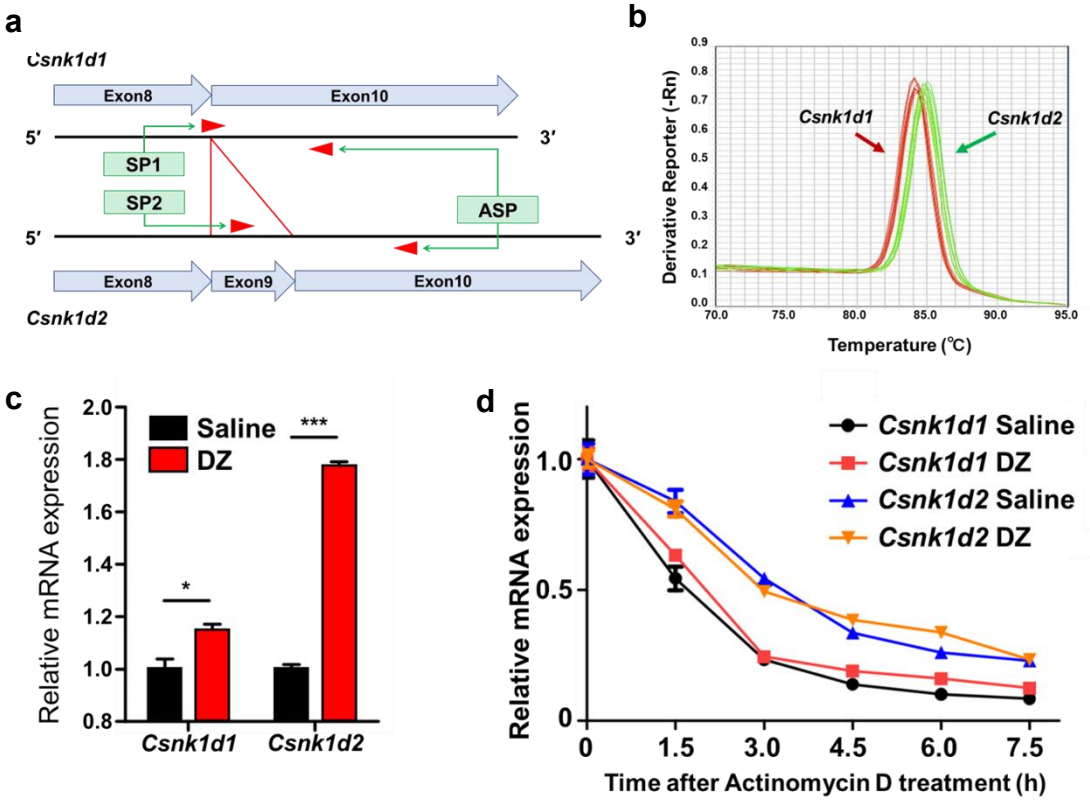

Fig. 6. Quantification of *Csnk1d* transcripts

(a) Designs of RT-qPCR primers for isoform-specific detection. The sense primer for *Csnk1d1* (SP1) was designed on the junction of Exon8 and Exon10, and the sense primer for *Csnk1d2* (SP2) was designed on Exon 9. Common Anti-sense primer (ASP) is designed on Exon 10. (b) Melting curves of RT-qPCR product amplified with isoform-specific primers. Red curves and green curves derive from amplicons of *Csnk1d1* and *Csnk1d2* respectively. (c) Result of RT-qPCR with isoform specific primers (n=9). Raw data were normalized by relative expression of *Rplp0*. Average value of each target in WT was set as 1 (error bars represent SEMs, **p*<0.05, ****p*<0.001). (d) Actinomycin D (5 μM) was added after 2 days treatment with 100 μM DZ. Sampling was conducted every 1.5 h after Actinomycin D treatment started. The mRNAs were quantified by RT-qPCR. For each target, first concentrations are set as 1. Error bars represents ± SEM (n=3).

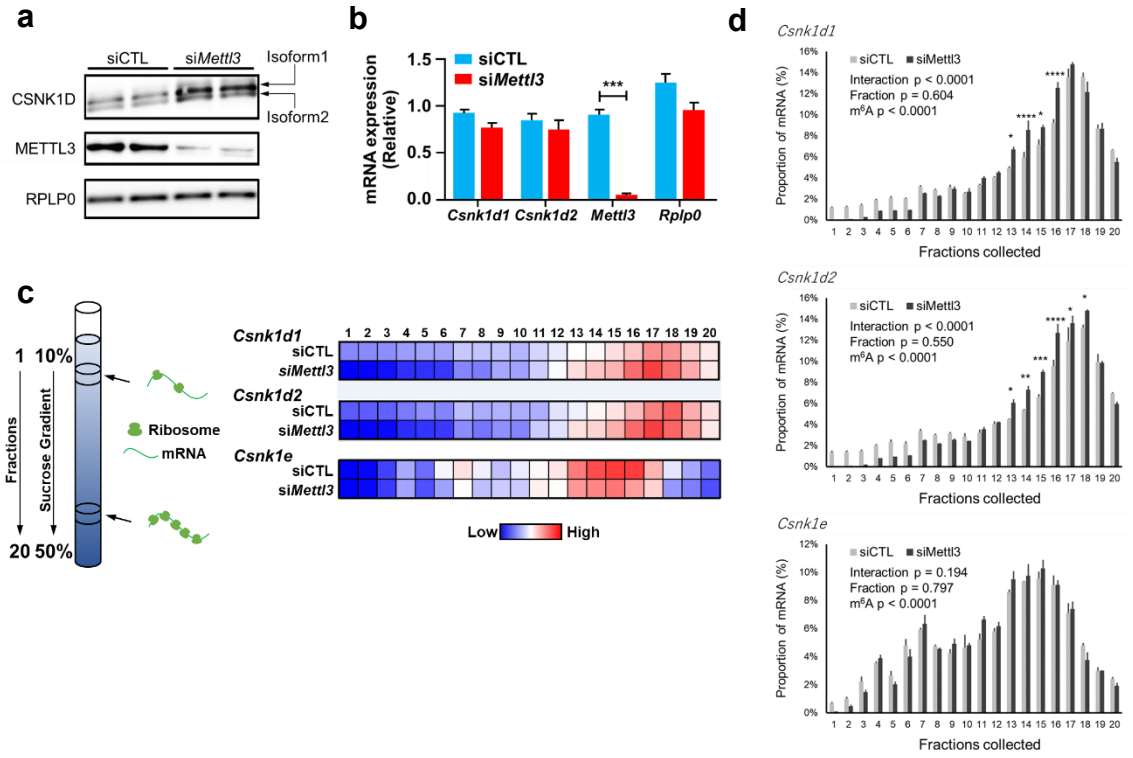

Fig. 7. CSNK1D expression is post-transcriptionally regulated by m^{6}A

(a) *Mettl3* silencing increases CSNK1D protein levels. Knock-down of METTL3 was confirmed by immunoblotting. RPLP0 was used as a loading control. (b) *Mettl3* silencing causes little changes on *Csnk1d* mRNA steady-state levels. Data are shown as mean ± SEM (n=4), analyzed by one-way ANOVA and Bonferroni post-t test. (***p<0.001) (c) Scheme of polysome profiling (left) and heatmap visualization of mean relative mRNA abundance (n=3) for each transcript in each fraction (right). *Mettl3* causes shift of the population of the *Csnk1d1* and *Csnk1d2* transcripts from lower to higher density fraction, indicating enhanced translation. This was not observed for *Csnk1e*, which has no significant m^{6}A peak. (d) Bar charts show mean ΔCT ± SEM of indicated transcripts in each fraction, with significance levels in two-way ANOVA followed by Bonferroni post hoc test, n = 3, *p<0.05, **p<0.01, ***p<0.001, ****p<0.0001.

Ablation of *Csnk1d* m^{6}A methylation by CRISPR-Cas9 in vivo

Next, to investigate the physiological role of the methylated locus in the 3′-UTR of *Csnk1d*, I generated a mutant mouse strain with a 43-bp deletion in the genomic region corresponding to the m^{6}A peak (**Figs. 2, 8a, and 8b**). This deletion does not affect the coding sequence but removes the *N*^{6}-methylated adenosine at GGm^{6}ACA, located previously by screening of m^{6}A sites in brain and liver transcriptomes [24].

The consequences of this mutation on *Csnk1d* m^{6}A levels, mRNA and protein expression were investigated in the liver, since it is known to have high mRNA m^{6}A levels in the liver [25]. As expected, *Csnk1d* transcripts had lower m^{6}A levels in −43/−43 animals compared with wild type (**Fig. 8c**), whereas neither of the *Csnk1d* mRNA levels was significantly affected like METTL3 silencing (**Fig. 8d**). In contrast, the CSNK1D protein levels increased significantly: homozygous −43 mutant mice had higher CSNK1D levels in the liver (**Fig. 8e**), and had a longer period (23.97 h ± 0.02) of locomotor activity behavior rhythms compared with wild-type mice (23.64 h ± 0.08, **Figs. 8f and 8g**). Although non-coding, this mutation, weakening m^{6}A-dependent post-transcriptional processes limiting CSNK1D expression, was sufficient to cause an observable increase in the CSNK1D proteins, accompanied by a change in circadian locomotor activity behavior.

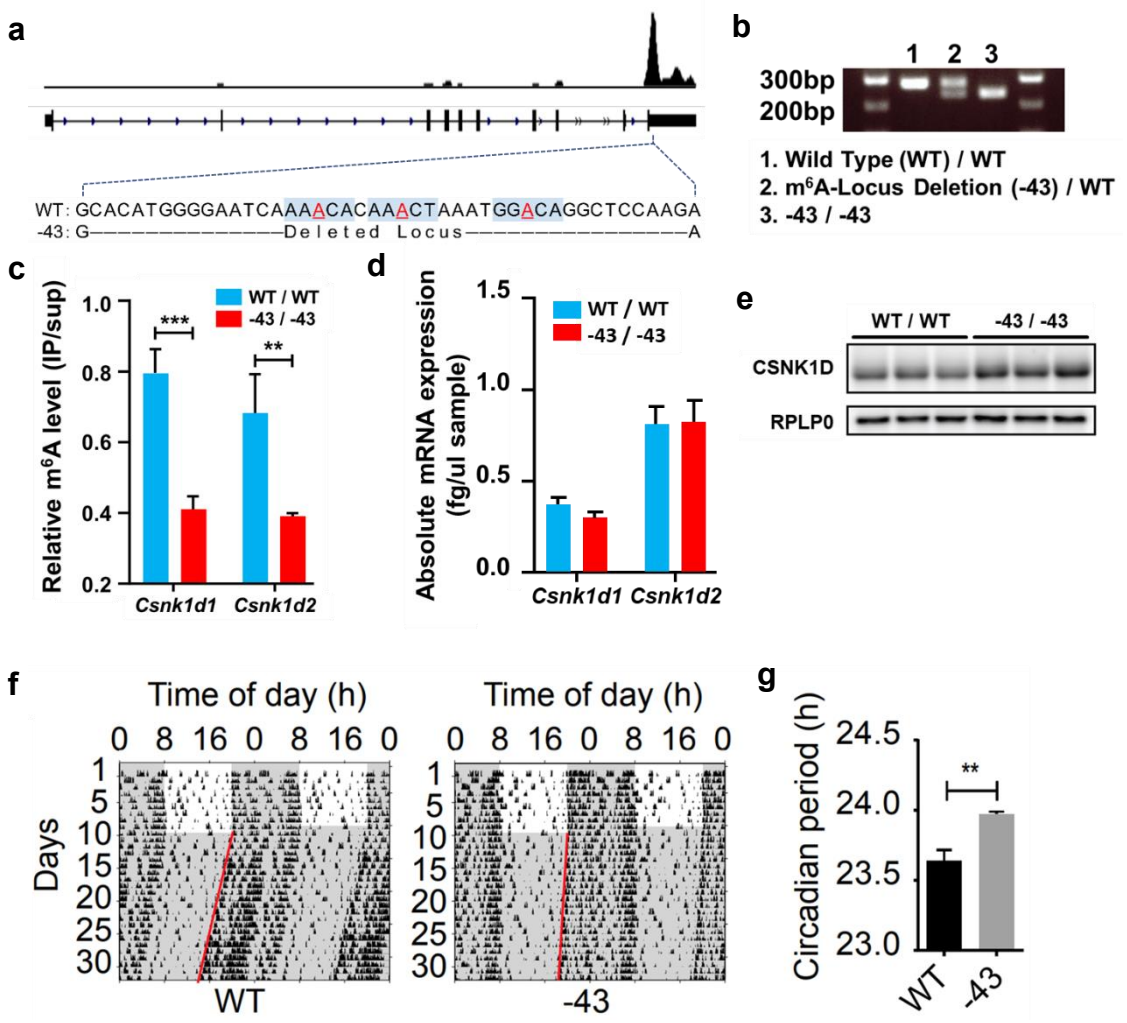

Fig. 8. Deletion of m^{6}A locus from *Csnk1d* 3′-UTR is sufficient to elongate the circadian period *in vivo*.

(a) Location of the mutation and genotyping of mice bearing a −43 deletion in the *Csnk1d* gene. The region of the zoomed m^{6}A peak corresponds to the peak summit identified by MACS2 peak calling analysis. (b) Results of genotyping. (c) Quantification of *Csnk1d* mRNA m^{6}A levels. (d) Quantification of *Csnk1d1* and *Csnk1d2* mRNA expression in the liver by qPCR. (c) and (d) were analyzed by two-way ANOVA (wild type vs. −43, ***p*<0.01, n = 3) followed by Bonferroni post hoc, ****p*<0.001. (e) Representative immunoblotting for CSNK1D and loading control RPLP0 with liver samples. (f) Circadian locomotor activity recording from one representative animal of each genotype is shown. (g) Period of circadian locomotor activity of each genotype was analyzed by χ^2 periodogram; mean period ± SEM was analyzed by Student t test of n=6 animals.

Discussion

Here, I revealed that one of the key circadian clock regulators, *Csnk1d*, is under m^6A-dependent regulation. This m^6A modification takes place on the 3′-UTR of the *Csnk1d* transcript and is sufficient to regulate the expression of the CSNK1D protein. The measurement of the locomotor activity of mice with m^6A locus deletion demonstrated that the m^6A locus is required for the proper oscillations of the circadian clock. While the lack of *Csnk1d* is embryonic lethal [20], higher expression or increased activity has been linked to cancer progression, migraine, and circadian disruption [26]. Thus, the significance of the negative regulation of CSNK1D expression by its methylated 3′-UTR goes beyond the circadian field, given the manifold functions of CSNK1D.

The mechanisms of CSNK1D induction by the broad methylation inhibitor (DZ) and RNA-methylation specific inhibition appear to be distinct. Although DZ-dependent induction of CSNK1D and changes in *Csnk1d* alternative splicing have not been fully explored in this thesis, there are several possibilities: (1) changes in histone methylation or DNA methylation alters transcription rate, accompanied by co-transcriptional splicing disfunction, (2) splicing-related proteins require methylation for proper functions to complete co-transcriptional splicing, and (3) inhibition of mRNA methylation (other than m^6A) affects co-transcriptional processes. Further investigation should reveal what methylation is responsible for CSNK1D induction by

DZ.

The stability of each *Csnk1d* isoform is quite different, despite 98.3% mRNA sequences are identical. Interestingly, a recent report shows each CSNK1D isoform exhibits different sub-cellular localization [27], further indicating the functional importance of Exon 9 of the *Csnk1d* gene. Future studies of this short but important exon might be useful to understand regulatory mechanism and molecular behavior of mRNAs.

Considering the case of METTL3 silencing and 43-bp deletion, it is likely that the "unknown translation inhibitor" binds to the methylation site of *Csnk1d* mRNA in an m^6A-dependent manner (**Fig. 9**). It is possible that the “unknown translation inhibitor” does not bind to m^6A directly, but bind to the proximal region denatured by m^6A. Consistent with this idea, several programs used for mRNA structure prediction have shown that the region containing the m^6A peak sequence of the *Csnk1d* mRNA forms a hairpin structure (**Fig. 10**).

Then, the next question is what is the "unknown translation inhibitor"? Looking at previous studies on the relationship between m^6A modification and translation, there are several proteins that affect translation efficiency (such as YTH domain-containing proteins) [28], but no protein has been reported to bind to the methylated 3′-UTR of target transcripts and repress translation. Future studies aimed at identifying "unknown translation inhibitors" will be of great worth in understanding the mechanisms of gene regulation governed by m^6A modification, as well as circadian

clock regulation by m^6A modification via alteration of CSNK1D expression.

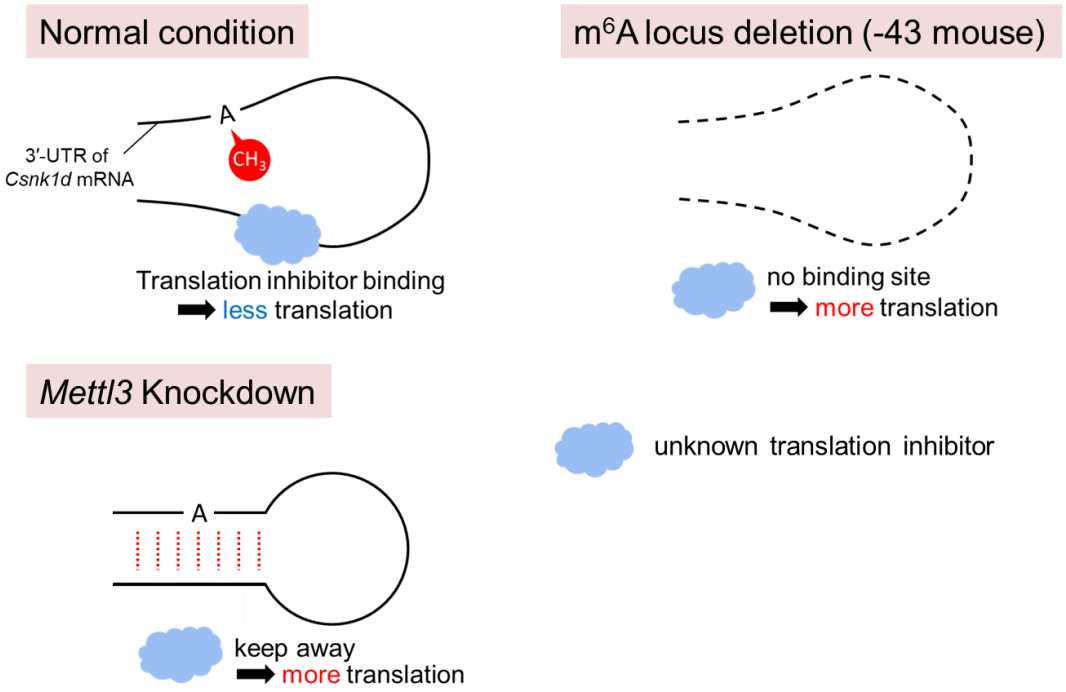

Fig. 9. Hypothesis of post-transcriptional *Csnk1d* regulation by m^{6}A

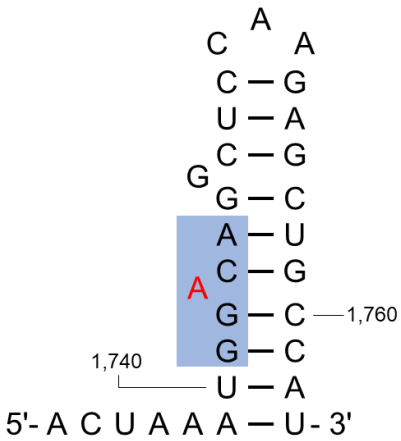

Fig. 10. Predicted local secondary structure of the *Csnk1d* 3′-UTR containing one putative m^{6}A site.

ViennaRNA, mfold and vsfold predicted same secondary structure for this region.
The number indicates position from 5′ end of the *Csnk1d2* transcript.

1. 2 Two alternative splicing isoforms of CSNK1D antagonistically controls speed of the circadian clock

Results

CSNK1D2 overexpression causes circadian period elongation.

According to the previous studies, induction of CSNK1D does not seem to trigger circadian period elongation. However, the results obtained by the DZ treatment, *in vitro* METTL3 silencing, and *in vivo* deletion of the *Csnk1d* m^6A locus all led to the induction of CSNK1D with circadian period elongation. To test whether an increase in CSNK1D triggers circadian period elongation, I decided to investigate the functional differences between the alternatively spliced isoforms of CSNK1D, which have not been characterized so far.

To reveal functional differences between the CSNK1D isoforms in circadian clock regulation, immortalized MEFs prepared from PERIOD2::LUCIFERASE knock-in reporter mice [29] (PER2::LUC MEFs) were stably transfected with an expression vector for CSNK1D1 or CSNK1D2 (**Fig. 11**). As expected, overexpression of CSNK1D1 increased the intensity of the upper band, while that of CSNK1D2 increased the lower band intensity (**Fig. 11 top**). Overexpression of CSNK1D1 in PER2::LUC MEFs led to a shorter period, in accordance with the previous study [23], compared with MEFs stably transfected with the empty vector. Intriguingly, CSNK1D2

overexpression led to approximately 1 h period elongation (**Fig. 11 bottom**). These results suggest that CSNK1D1 and CSNK1D2 control the circadian clock in the opposite direction.

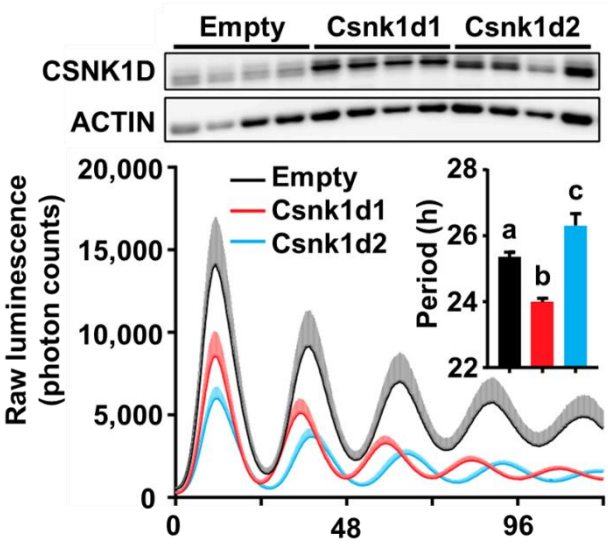

Fig. 11. Effects of overexpression of CSNK1D isoforms on the circadian period.

Stable overexpression of CSNK1D1 and CSNK1D2 in PER2::LUC MEFs leads to period shortening and lengthening, respectively. (Inset) Period analyzed by one-way ANOVA, $p<0.001$, with a vs. b vs. c in Bonferroni post hoc at least $p<0.05$; results shown are mean ± SEM of n = 4 monoclonal cell lines for each group. (Top) CKSN1D and ACTIN immunoblots for each cell line.

CSNK1D2-specific knockdown causes period shortening.

To further investigate the functional difference between the CSNK1D isoforms, CSNK1D2-specific knockdown in PER2::LUC MEFs was performed using siRNA targeting Exon 9 (**Fig. 12**). The intensity of the lower CSNK1D band was considerably reduced by transfection of siRNA targeting Exon 9, indicating successful knockdown of CSNK1D2 without affecting the CSNK1D1 level (**Fig. 12 top**). The selective CSNK1D2 knockdown shortened the circadian period, which was opposite to nonselective knockdown of both CSNK1D1 and CSNK1D2 (**Fig. 12 bottom**). These results indicate that CSNK1D1 and CSN1KD2 differentially regulate the circadian clock, probably in an antagonistic manner.

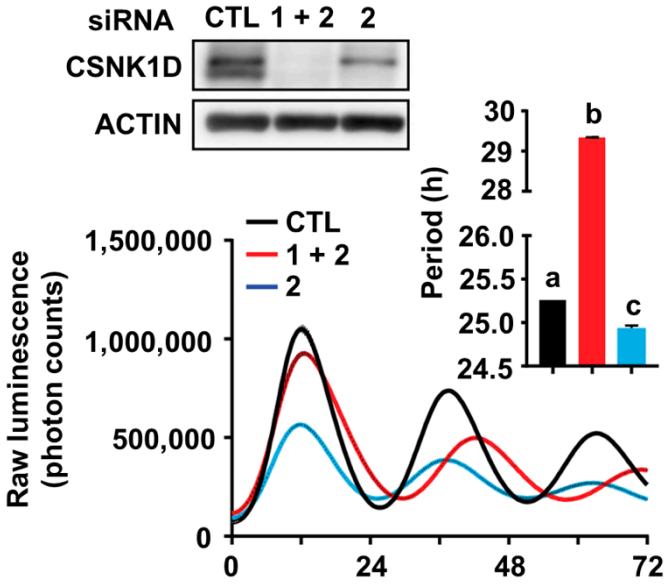

Fig. 12. Knockdown of *Csnk1d* isoforms.

Silencing of *Csnk1d2* in PER2::LUC MEFs leads to short period, while silencing of both *Csnk1d*s leads to long period. Knockdown efficiency of *Csnk1d* and *Csnk1d2* was first confirmed by immunoblotting (Top). Main graph shows mean ± SEM of real-time luminometry traces for each group; n = 2. (Right Inset) Mean period ± SEM analyzed by one-way ANOVA, $p<0.0001$. a vs. b vs. c, at least $p< 0.01$ in Bonferroni post hoc.

Discussion

Previous studies indicated that increased expression of CSNK1D does not cause elongation of the period of the circadian clock [20-23]. However, I here found that the non-canonical isoform, CSNK1D2, lengthens the circadian period, which is opposite to what was known about the canonical isoform CSNK1D1. Together with the results obtained in this study, it is suggested that the m^6A modification differentially regulates translation of two *Csnk1d* mRNAs generated via alternative splicing, and the opposing activities of the two CSNK1D isoforms allow complex regulation of the speed of the circadian clock (**Fig. 13**).

Most studies have reported that inhibition or reduction of CSNK1D increased the period length of the circadian clock. On the other hand, studies on familial advanced sleep phase syndrome 1 (FASPS1) have suggested implication of CSNK1D in period shortening. FASPS1 is characterized by very early sleep onset and offset due to the PER2 S662G mutation [30, 31], which is explained by the destabilization of PER2. Phosphorylation at S662 by an unknown priming kinase is known to stabilize PER2 by promoting subsequent phosphorylation at a downstream residue called the FASPS site by CSNK1D [32]. Thus, the PER2 S662G mutant is less stable because of the lack of phosphorylation at the FASPS site.

Therefore, the FASPS site alone is not able to explain the results of previous studies showing that reduction or inhibition of CSNK1D prolongs the circadian clock cycle. In

fact, CSNK1D can phosphorylate other residues in PER2, and it is known that phosphorylation of these residues promotes the degradation of PER2 [33]. Taken together with the results obtained in this study, it is speculated that CSNK1D2 phosphorylates the FASPS site preferentially over CSNK1D1 and contributes to the stabilization of PER2. On the contrary, it is speculated that CSNK1D1 destabilizes PER2 mainly by phosphorylating other residues (**Fig. 13**).

The significance of the antagonistic activities of the CSNK1D isoforms is thought to lie in the link between alternative splicing and the regulation of the circadian clock. Since alternative splicing is known to be regulated by a variety of extracellular stimuli [34], these stimuli may affect the speed of the circadian clock through regulating the *Csnk1d* alternative splicing. It is therefore interesting to investigate the effects of daily variations in body temperature and neural activity on the alternative splicing of *Csnk1d*.

CSNK1D plays an important role in a very wide range of physiological processes, and the importance of the functional differences between the CSNK1D isoforms revealed in this study is not limited to the field of circadian clock studies. An issue to be addressed in the future studies is the relationship between the phosphorylation activities and physiological functions of the CSNK1D isoforms.

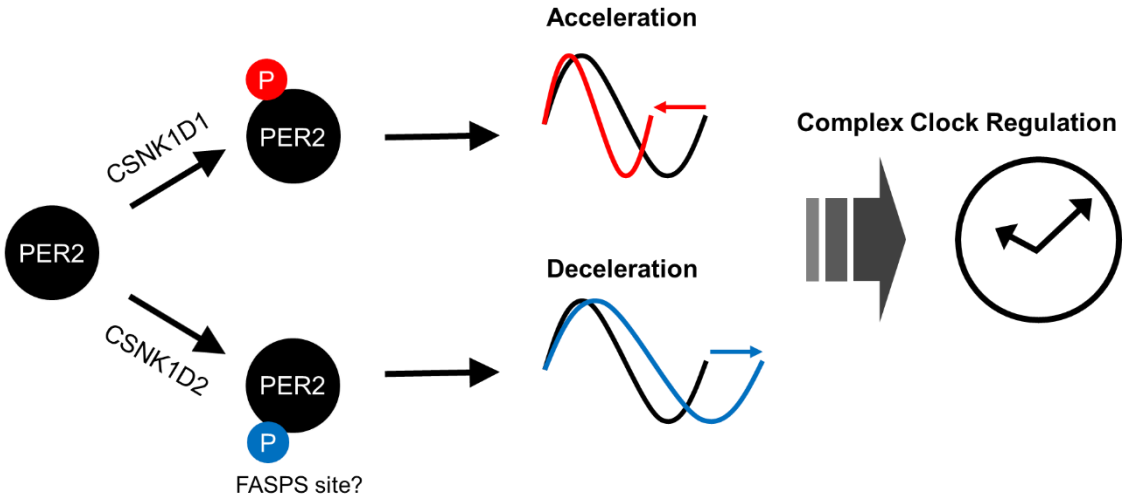

Fig. 13. Antagonistic functions of two CSNK1D isoforms allow complex circadian clock regulation.

Reference

1. Lee, Y., & Rio, D. C. (2015). Mechanisms and regulation of alternative Pre-mRNA splicing. Annual Review of Biochemistry, 84, 291–323. https://doi.org/10.1146/annurev-biochem-060614-034316

2. Cantara, W. A., Crain, P. F., Rozenski, J., McCloskey, J. A., Harris, K. A., Zhang, X., Vendeix, F. A. P., Fabris, D., & Agris, P. F. (2011). The RNA modification database, RNAMDB: 2011 update. Nucleic Acids Research, 39(SUPPL. 1), 195–201. https://doi.org/10.1093/nar/gkq1028

3. Boccaletto, P., MacHnicka, M. A., Purta, E., Pitkowski, P., Baginski, B., Wirecki, T. K., De Crécy-Lagard, V., Ross, R., Limbach, P. A., Kotter, A., Helm, M., & Bujnicki, J. M. (2018). MODOMICS: A database of RNA modification pathways. 2017 update. Nucleic Acids Research, 46(D1), D303–D307. https://doi.org/10.1093/nar/gkx1030

4. Yue, Y., Liu, J., & He, C. (2015). RNA N6-methyladenosine methylation in post-transcriptional gene expression regulation. Genes and Development, 29(13), 1343–1355. https://doi.org/10.1101/gad.262766.115

5. Liu, J., Yue, Y., Han, D., Wang, X., Fu, Y., Zhang, L., Jia, G., Yu, M., Lu, Z., Deng, X., Dai, Q., Chen, W., & He, C. (2014). A METTL3-METTL14 complex mediates mammalian nuclear RNA N6-adenosine methylation. Nature Chemical Biology, 10(2), 93–95. https://doi.org/10.1038/nchembio.1432

6. Wang, X., Lu, Z., Gomez, A., Hon, G. C., Yue, Y., Han, D., Fu, Y., Parisien, M., Dai, Q., Jia, G., Ren, B., Pan, T., & He, C. (2014). N 6-methyladenosine-dependent regulation of messenger RNA stability. Nature, 505(7481), 117–120. https://doi.org/10.1038/nature12730

7. Zheng, G., Dahl, J. A., Niu, Y., Fedorcsak, P., Huang, C. M., Li, C. J., Vågbø, C. B., Shi, Y., Wang, W. L., Song, S. H., Lu, Z., Bosmans, R. P. G., Dai, Q., Hao, Y. J., Yang, X., Zhao, W. M., Tong, W. M., Wang, X. J., Bogdan, F., … He, C. (2013). ALKBH5 Is a Mammalian RNA Demethylase that Impacts RNA Metabolism and Mouse Fertility. Molecular Cell, 49(1), 18–29. https://doi.org/10.1016/j.molcel.2012.10.015

8. Batista, P. J., Molinie, B., Wang, J., Qu, K., Zhang, J., Li, L., Bouley, D. M., Lujan, E., Haddad, B., Daneshvar, K., Carter, A. C., Flynn, R. A., Zhou, C., Lim, K. S., Dedon, P., Wernig, M., Mullen, A. C., Xing, Y., Giallourakis, C. C., & Chang, H. Y. (2014). M6A RNA modification

controls cell fate transition in mammalian embryonic stem cells. Cell Stem Cell, 15(6), 707–719. https://doi.org/10.1016/j.stem.2014.09.019

9. Patil, D. P., Chen, C. K., Pickering, B. F., Chow, A., Jackson, C., Guttman, M., & Jaffrey, S. R. (2016). M6 A RNA methylation promotes XIST-mediated transcriptional repression. Nature, 537(7620), 369–373. https://doi.org/10.1038/nature19342

10. Ries, R. J., Zaccara, S., Klein, P., Olarerin-George, A., Namkoong, S., Pickering, B. F., Patil, D. P., Kwak, H., Lee, J. H., & Jaffrey, S. R. (2019). m6A enhances the phase separation potential of mRNA. Nature, 571(7765), 424–428. https://doi.org/10.1038/s41586-019-1374-1

11. Fustin, J. M., Doi, M., Yamaguchi, Y., Hida, H., Nishimura, S., Yoshida, M., Isagawa, T., Morioka, M. S., Kakeya, H., Manabe, I., & Okamura, H. (2013). XRNA-methylation-dependent RNA processing controls the speed of the circadian clock. Cell, 155(4), 793. https://doi.org/10.1016/j.cell.2013.10.026

12. Partch, C. L., Green, C. B., & Takahashi, J. S. (2014). Molecular architecture of the mammalian circadian clock. Trends in Cell Biology, 24(2), 90–99. https://doi.org/10.1016/j.tcb.2013.07.002

13. Hardin, P. E., Hall, J. C., & Rosbash, M. (1990). Feedback of the Drosophila period gene product on circadian cycling of its messenger RNA levels. Nature, 343(6258), 536–540. https://doi.org/10.1038/343536a0

14. Zheng, B., Larkin, D. W., Albrecht, U., Sun, Z. S., Sage, M., Eichele, G., Lee, C. C., & Bradley, A. (1999). The mPer2 gene encodes a functional component of the mammalian circadian clock. Nature, 400(6740), 169–173. https://doi.org/10.1038/22118

15. Cheon, S., Park, N., Cho, S., & Kim, K. (2013). Glucocorticoid-mediated Period2 induction delays the phase of circadian rhythm. Nucleic Acids Research, 41(12), 6161–6174. https://doi.org/10.1093/nar/gkt307

16. Eide, E. J., Woolf, M. F., Kang, H., Woolf, P., Hurst, W., Camacho, F., Vielhaber, E. L., Giovanni, A., & Virshup, D. M. (2005). Control of Mammalian Circadian Rhythm by CKIε-Regulated Proteasome-Mediated PER2 Degradation. Molecular and Cellular Biology, 25(7), 2795–2807. https://doi.org/10.1128/mcb.25.7.2795-2807.2005

17. Petronczki, M., Matos, J., Mori, S., Gregan, J., Bogdanova, A., Schwickart, M., Mechtler, K., Shirahige, K., Zachariae, W., &

Nasmyth, K. (2006). Monopolar Attachment of Sister Kinetochores at Meiosis I Requires Casein Kinase 1. Cell, 126(6), 1049–1064. https://doi.org/10.1016/j.cell.2006.07.029

18. Behrend, L., Milne, D. M., Stöter, M., Deppert, W., Campbell, L. E., Meek, D. W., & Knippschild, U. (2000). IC261, a specific inhibitor of the protein kinases casein kinase 1-delta and -epsilon, triggers the mitotic checkpoint and induces p53-dependent postmitotic effects. Oncogene, 19(47), 5303–5313. https://doi.org/10.1038/sj.onc.1203939

19. Ghalei, H., Schaub, F. X., Doherty, J. R., Noguchi, Y., Roush, W. R., Cleveland, J. L., Elizabeth Stroupe, M., & Karbstein, K. (2015). Hrr25/CK1δ-directed release of Ltv1 from pre-40S ribosomes is necessary for ribosome assembly and cell growth. Journal of Cell Biology, 208(6), 745–759. https://doi.org/10.1083/jcb.201409056

20. Etchegaray, J.-P., Machida, K. K., Noton, E., Constance, C. M., Dallmann, R., Di Napoli, M. N., DeBruyne, J. P., Lambert, C. M., Yu, E. A., Reppert, S. M., & Weaver, D. R. (2009). Casein Kinase 1 Delta Regulates the Pace of the Mammalian Circadian Clock. Molecular and Cellular Biology, 29(14), 3853–3866. https://doi.org/10.1128/mcb.00338-09

21. Lee, J. W., Hirota, T., Peters, E. C., Garcia, M., Gonzalez, R., Cho, C. Y., Wu, X., Schultz, P. G., & Kay, S. A. (2011). A small molecule modulates circadian rhythms through phosphorylation of the period protein. Angewandte Chemie - International Edition, 50(45), 10608–10611. https://doi.org/10.1002/anie.201103915

22. Isojima, Y., Nakajima, M., Ukai, H., Fujishima, H., Yamada, R. G., Masumoto, K. H., Kiuchi, R., Ishida, M., Ukai-Tadenuma, M., Minami, Y., Kito, R., Nakao, K., Kishimoto, W., Yoo, S. H., Shimomura, K., Takao, T., Takano, A., Kojima, T., Nagai, K., … Ueda, H. R. (2009). CKIε/δ-dependent phosphorylation is a temperature-insensitive, period-determining process in the mammalian circadian clock. Proceedings of the National Academy of Sciences of the United States of America, 106(37), 15744–15749. https://doi.org/10.1073/pnas.0908733106

23. Lee, H., Chen, R., Lee, Y., Yoo, S., & Lee, C. (2009). Essential roles of CKIδ and CKIε in the mammalian circadian clock. Proceedings of the National Academy of Sciences of the United States of America, 106(50), 21359–21364. https://doi.org/10.1073/pnas.0906651106

24. Ke, S., Alemu, E. A., Mertens, C., Gantman, E. C., Fak, J. J., Mele, A., Haripal, B., Zucker-Scharff, I., Moore, M. J., Park, C. Y., Vågbø, C.

B., Kuśnierczyk, A., Klungland, A., Darnell, J. E., & Darnell, R. B. (2015). A majority of m6A residues are in the last exons, allowing the potential for 3' UTR regulation. Genes and Development, 29(19), 2037–2053. https://doi.org/10.1101/gad.269415.115

25. Meyer, K. D., Saletore, Y., Zumbo, P., Elemento, O., Mason, C. E., & Jaffrey, S. R. (2012). Comprehensive analysis of mRNA methylation reveals enrichment in 3′ UTRs and near stop codons. Cell, 149(7), 1635–1646. https://doi.org/10.1016/j.cell.2012.05.003

26. Knippschild, U., Krüger, M., Richter, J., Xu, P., Balbina García-Reyes, Peifer, C., Halekotte, J., Bakulev, V., & Bischof, J. (2014). The CK1 family: Contribution to cellular stress response and its role in carcinogenesis. Frontiers in Oncology, 4 MAY(May), 1–32. https://doi.org/10.3389/fonc.2014.00096

27. Fazal, F. M., Han, S., Parker, K. R., Kaewsapsak, P., Xu, J., Boettiger, A. N., Chang, H. Y., & Ting, A. Y. (2019). Atlas of Subcellular RNA Localization Revealed by APEX-Seq. Cell, 178(2), 473-490.e26. https://doi.org/10.1016/j.cell.2019.05.027

28. Yoo, S. H., Yamazaki, S., Lowrey, P. L., Shimomura, K., Ko, C. H., Buhr, E. D., Siepka, S. M., Hong, H. K., Oh, W. J., Yoo, O. J.,

Menaker, M., & Takahashi, J. S. (2004). PERIOD2::LUCIFERASE real-time reporting of circadian dynamics reveals persistent circadian oscillations in mouse peripheral tissues. Proceedings of the National Academy of Sciences of the United States of America, 101(15), 5339–5346. https://doi.org/10.1073/pnas.0308709101

29. Jones, C. R., Campbell, S. S., Zone, S. E., Cooper, F., Desano, A., Murphy, P. J., Jones, B., Czajkowski, L., & Ptáček, L. J. (1999). Familial advanced sleep-phase syndrome: A short-period circadian rhythm variant in humans. Nature Medicine, 5(9), 1062–1065. https://doi.org/10.1038/12502

30. Toh, K. L., Jones, C. R., He, Y., Eide, E. J., Hinz, W. A., Virshup, D. M., Ptáček, L. J., & Fu, Y. H. (2001). An hPer2 phosphorylation site mutation in familial advanced sleep phase syndrome. Science, 291(5506), 1040–1043. https://doi.org/10.1126/science.1057499

31. Shanware, N. P., Hutchinson, J. A., Kim, S. H., Zhan, L., Bowler, M. J., & Tibbetts, R. S. (2011). Casein kinase 1-dependent phosphorylation of familial advanced sleep phase syndrome-associated residues controls PERIOD 2 stability. Journal of Biological Chemistry, 286(14), 12766–12774. https://doi.org/10.1074/jbc.M111.224014

32. Shirogane, T., Jin, J., Ang, X. L., & Harper, J. W. (2005). SCFβ-TRCP controls Clock-dependent transcription via casein kinase 1-dependent degradation of the mammalian period-1 (Per1) protein. Journal of Biological Chemistry, 280(29), 26863–26872. https://doi.org/10.1074/jbc.M502862200

33. Zaccara, S., Ries, R. J., & Jaffrey, S. R. (2019). Reading, writing and erasing mRNA methylation. Nature Reviews Molecular Cell Biology, 20(10), 608–624. https://doi.org/10.1038/s41580-019-0168-5

34. Naftelberg, S., Schor, I. E., Ast, G., & Kornblihtt, A. R. (2015). Regulation of Alternative Splicing Through Coupling with Transcription and Chromatin Structure. Annual Review of Biochemistry, 84(1), 165–198. https://doi.org/10.1146/annurev-biochem-060614-034242

Chapter 2

Improved automated void stain on paper (aVSOP) system for simultaneous recording of micturition and locomotor behavior

Introduction

In mammals, most organs have an ability to generate circadian rhythms that coordinate various physiological phenomena [4, 19]. This basic clock mechanism, composed of clock genes interlocked in transcription-translation feedback loops in which Period genes (*Per1*, *Per2* and *Per3*) play a central role, exists in virtually all cells in the body [5, 11, 13]. The circadian rhythms in all cells are synchronized by the master clock in the hypothalamic suprachiasmatic nucleus (SCN). Through this synchronization, the SCN drives rhythms in physiologically relevant phenomena such as body temperature and blood pressure [10, 15, 25]. The SCN also engages in entraining rhythms to the environmental light-dark cycles, so that endogenous circadian rhythms are normally entrained to the ambient solar time. However, when traveling across multiple time zones, the internal clock shows temporal desynchronization with the external solar time [6, 12]. This desynchronization evokes jet lag symptoms, including sleep disturbances and gastrointestinal distress [3, 14], although their precise pathophysiology has been unexplored.

As an important physiological function, micturition behavior also shows circadian rhythms. The increase of urine production in the kidneys and the decrease of storage capacity of the urinary bladder drive micturition. In a healthy person, urine production is reduced and urine storage capacity is increased at night for a sound sleep [7, 21, 23]. Nocturnal enuresis in children and nocturia in the elderly are speculated to be

caused by a mismatch between urine production rate in the kidneys and storage capacity of the urinary bladder [20, 22]. In jet lag, frequent micturition often disturbs sleep, since the internal clock cannot be instantly reset to local time but continues to oscillate autonomously on its own time for several cycles. However, until now, implication of circadian rhythm in day/night micturition behaviors in jet lag, has not been established.

Since mice are nocturnal, micturition occurs more often at night, but its accurate frequency and volume have not been quantified so far because of the minute urine volume voided per micturition [18, 24]. Recently, Negoro *et al*. [8] succeeded to record circadian micturition rhythms in free-moving mice by the automated Voided Stain on Paper (aVSOP) method, which can accurately record micturition of mice. In the present study, I examined the disrupted micturition rhythms during jet-lag by an improved aVSOP method, which enables to record micturition rhythms and behavioral rhythms simultaneously. I examined the change of the micturition rhythm not only in wild-type (WT) mice, but also in *Per*-null (*Per1*, *Per2*, and *Per3* knockout) mice whose clock oscillation is disrupted.

Materials and Methods

Animals

Male *Per*-null mice (*Per1*$^{-/-}$, *Per2*$^{-/-}$, and *Per3*$^{-/-}$) [1] and wild-type Balb/c mice (WT) aged 10–16 weeks were used. We generated *Per*-null mice by crossing *Per1*-knockout [1], *Per2* Brdm1-mutant [29], and *Per3*-knockout [16] mice, on the BALB/c strain with backcrosses for at least 10 generations [1]. Mice were housed individually in wire net cages (5.0 mm × 5.0 mm square net with wire diameter 0.7 mm) with ad libitum access to food and water. The animals were treated in accordance with the ethical guidelines of the Kyoto University Animal Experimentation Committee.

Measurement of behavioral and micturition rhythms.

Per-null and WT mice were entrained to a 12-h-light (~200 lux fluorescent light)/12-h-dark (LD) cycle at least two weeks to entrain the circadian clock of the mice to the ambient LD cycle, and then LD cycles were 8-h phase-advanced. Locomotor activity was recorded in 5-min bins with passive infrared sensor, and the data obtained were analysed with Clocklab software (Actimetrics) developed on MatLab (Mathworks). Micturition was recorded by using the aVSOP method. Rolled laminated filter paper, pre-treated to turn the edge of urine stains deep purple, was wound up at a speed of 5 cm per hour under a water-repellent wire lattice. Each urine stain was traced, scanned and quantified by Image J 1.42 software to convert micturition volume using

the formula of standard curve. Both locomotor activity and micturition rhythms were measured for 5 days under LD condition, followed by 14 days after the phase advance. Total urine volume per hour was estimated by dividing the volume by the time interval between the given and preceding voiding (filling time), when the filling time was more than 1 h [21]. Compared to our previous report using the aVSOP system [8], the dimensions of the mouse support wire lattice were optimized, reducing the size of holes to improve ambulatory stress.

Results

Simultaneous measurement of locomotor activity and micturition rhythms

In the improved aVSOP system of our laboratory (**Fig. 14a**), urine at each micturition was automatically collected on a blotting paper scroll moving at a constant low speed just under the animal cage equipped with a wire bottom (**Fig. 14b**). To generate a standard formula to show the correlation of liquid volume and stained area of a dot on filter paper, a standard curve with normal saline ranging from 10 to 800 μL was blotted on a filter paper (**Fig. 14c**). I scanned and quantified these saline stains, and found a clear linear correlation between poured volume and the stained area ranging from 10–800 μL.

When animals were housed in LD conditions, WT mice showed a higher locomotor activity in the night time than in the day time (**Fig. 15a**). Similar to the locomotor activity, the micturition frequency of WT mice was higher in night time (6.25 ± 0.78 times/12 h, n = 5) than in day time (0.542 ± 0.152 times/12 h, n = 5) (**Fig. 15b**). Similarly, the total void volume per hour also showed an increase in night time (**Fig. 15c**). In *Per*-null mice whose circadian clock is completely disrupted, locomotor activity was high in the night time, and low in the day time as reported previously [2]. Similarly, the micturition frequency and void volume of micturition of *Per*-null mice showed temporal variation under LD cycles (**Figs. 15 and 15b**). Under LD conditions, however, this rhythmic

micturition is not driven by the endogenous clock, but is caused by the direct inhibition of locomotor activity by external light.

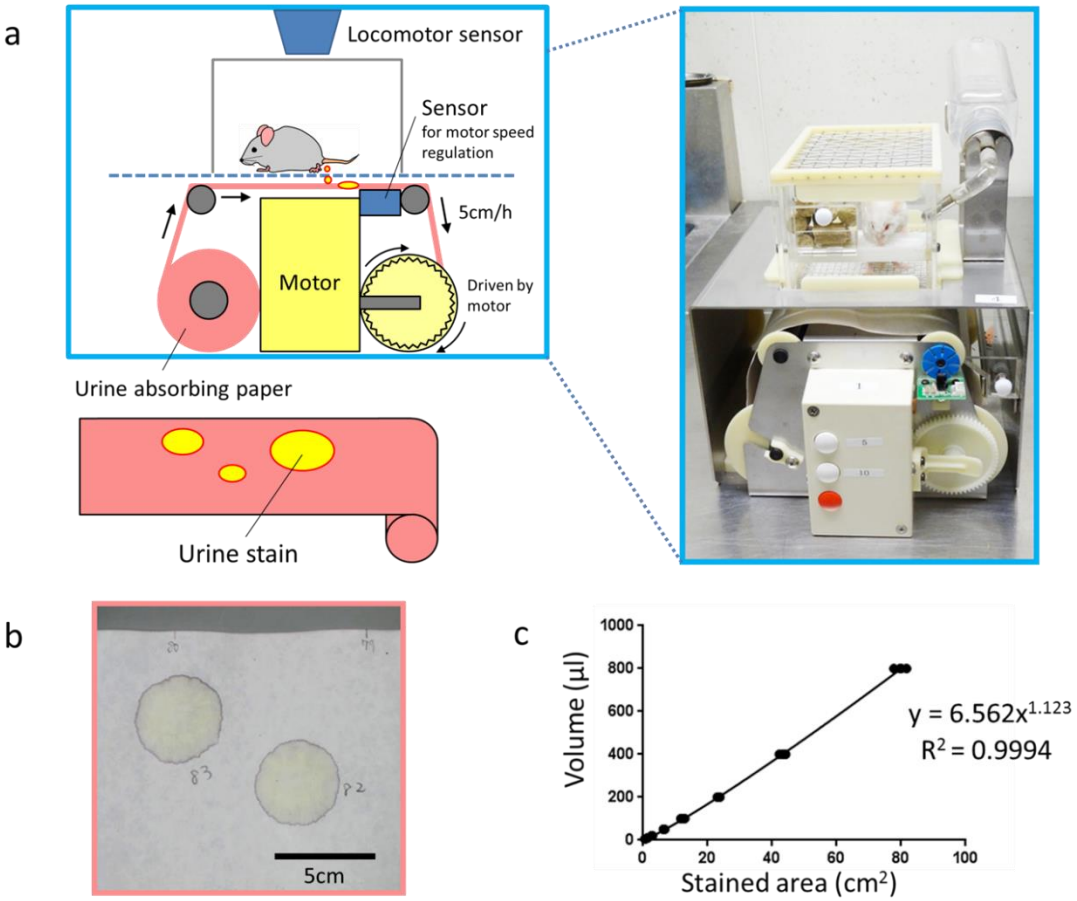

Fig. 14. Improved aVSOP system

(a) Diagram and real picture of an improved aVSOP system. An improved aVSOP system can measure the locomotor activity by the infrared sensor in addition to micturition volume.

(b) An example of urine spots on paper was shown. Motor drives paper at the speed of 5 cm/h (Bar =1 hour).

(c) Each urine dot on papers was traced, scanned and quantified by Image J 1.42 software. A standard curve was constructed from 10 to 800 µl of normal saline and their corresponding stained areas (n=3 for each volume).

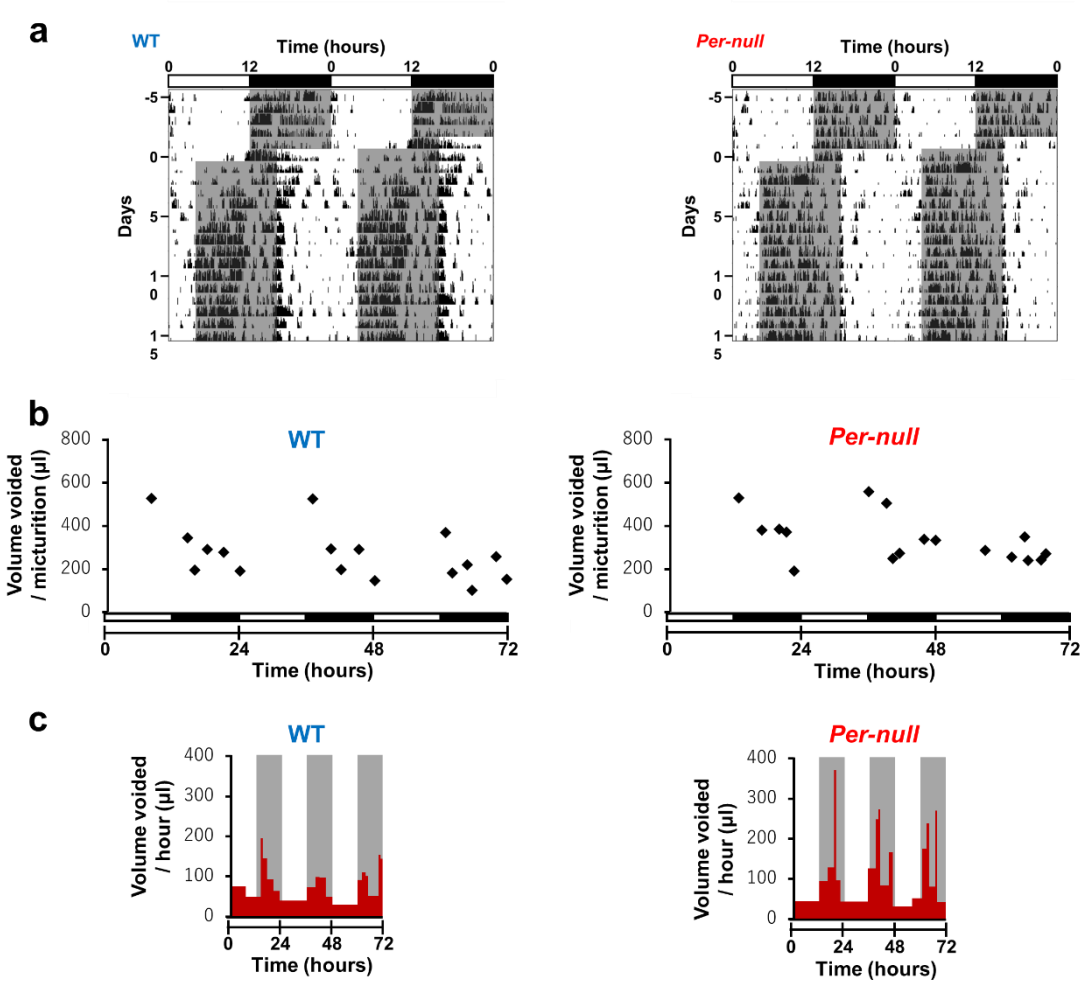

Fig. 15. Micturition rhythms of WT and *Per-null* mice under LD cycles

(a) Representative double plotted actogram of WT mice in LD condition, which is later subjected to an 8-hour phase advance in LD cycles. The advance was conducted on day 6. Top bars correspond with initial LD setting and shades indicate dark phases.

(b) Representative charts of urine volume voided per micturition of WT (top) and *Per-null* (bottom) mice under 12L12D cycles for 3days. White and black bars indicate light phase and dark phase respectively. Note that urination occurred mostly in the night time in both genotypes.

(c) Volume voided per hour was obtained by following calculation using data shown in figure (a). Here I define T(n) as the time when Nth urination occurred, V(n) as the urine volume of Nth urination, and V(t) as the value plotted in figure (b). Each value was rounded down to the nearest decimal. If T(n) and T(n-1) were equal, these two events were regarded as one event, so volume was added up.

$$V(t) = V(n) / \{T(n) - T(n-1)\} \quad , T(n-1) \quad < t \leqq T(n)$$

Locomotor activity and micturition rhythms in jet-lag

Next, I examined the locomotor activity and the urine volume voided per micturition simultaneously, under experimental jet lag conditions in WT and *Per*-null mice (**Fig. 16a**). In WT mice, urination showed temporal desynchronization from environmental LD cycles for several days after jet-lag similar to locomotor activity rhythms. In contrast, urination of *Per*-null mice tended to abruptly entrain to the environmental LD cycles, as observed from their locomotor activity rhythms (**Figs. 15a and 16a**). However, because micturition occurred inconsistently, often with several hours intervals, I found it difficult to quantitatively measure the re-entrainment speed of WT and mutant mice based on the observed changes in voided volume and micturition timing (**Fig. 16a**).

To overcome this problem, I quantified the estimated urine production per hour (**Fig. 16b**) by dividing the void volume by the time interval between the given and preceding voidings [21]; the data were also displayed in double-plot format for the comparison with that of locomotor activity rhythm (**Fig. 17a**). In WT mice, an 8-hour phase advance evoked a gradual shift of locomotor activity rhythms and micturition rhythms, and it took 6 to 8 days for complete re-entrainment to the new LD schedule. In contrast, *Per*-null mice showed almost immediate re-entrainment with only 2 to 4 days of transition (**Figs. 17a and 17b**). In both genotypes, there was no apparent discrepancy between re-entrainment of micturition and of locomotor activity.

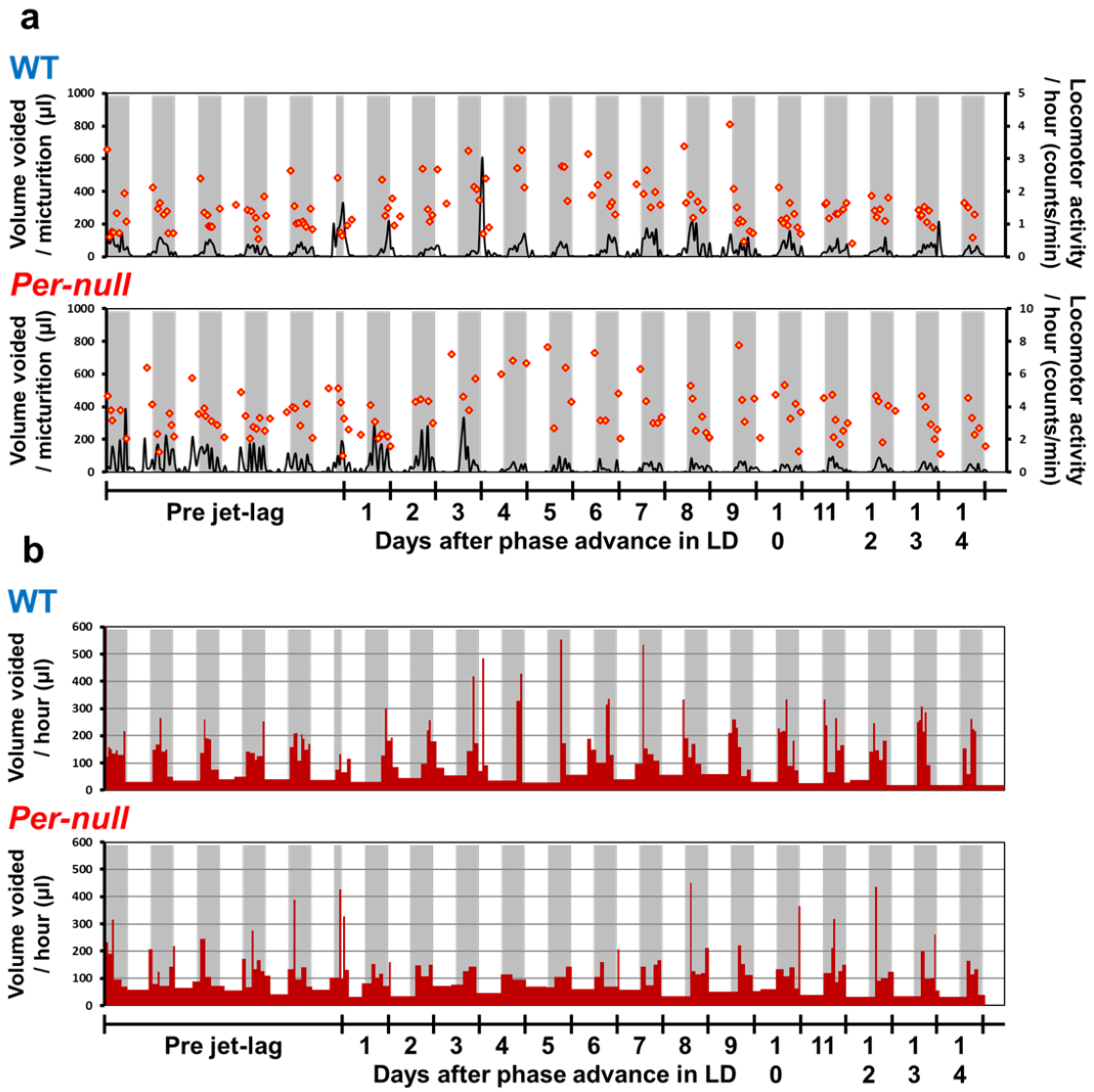

Fig. 16. Simultaneous measurement of locomotor activity and micturition rhythms of WT and *Per-null* mice under jet-lag conditions

(a) Representative charts of urine volume voided per micturition (orange diamonds) and locomotor activity per hour (black line) of WT (top) and *Per-null* (bottom) mice under jet-lag conditions.

(b) Total urine volume voided per hour of WT (top) and *Per-null* (bottom) mice under jet-lag conditions.

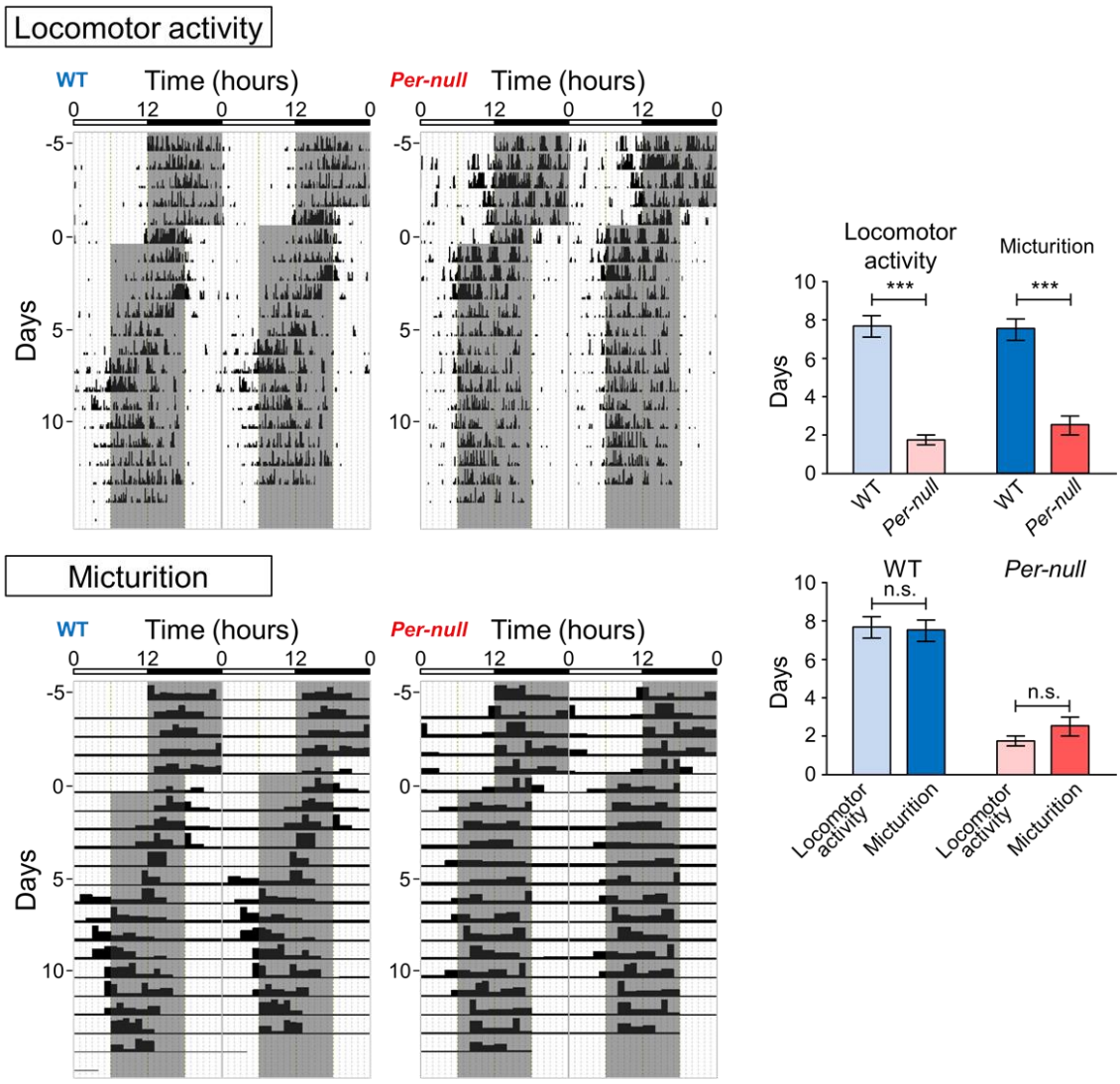

Fig. 17. Simultaneous measurement of locomotor activity and micturition rhythms of WT and *Per-null* mice under jet-lag conditions

(a) Representative charts of urine volume voided per micturition (orange diamonds) and locomotor activity per hour (black line) of WT (top) and *Per-null* (bottom) mice under jet-lag conditions.

(b) Total urine volume voided per hour of WT (top) and *Per-null* (bottom) mice under jet-lag conditions.

Discussion

The present study demonstrated that it takes about a week for complete entrainment of micturition, as well as locomotor activity, to the 8-h phase advance of LD cycles. Since the temporal desynchronization with the external solar time under this jet-lag schedule is similar to trans-meridian flights, mice can be used as a model for analyzing disrupted rhythms, although the day-night change is inverted because mice are nocturnal.

The production of urine by the kidneys, and the storage of urine in the urinary bladder are key steps in micturition [27]. Importantly, the regulation of storage or voiding of the urine depends on central as well as peripheral autonomic and somatic neural pathways, which receive higher-level regulatory input from various brain and spinal cord nuclei [28]. Since clock genes are expressed in virtually most cells of the body [14, 22], the biological clock may intrinsically regulate micturition by acting on any, if not all, of these control centers. Moreover, these structures indirectly receive circadian input from the master clock in the hypothalamic suprachiasmatic nucleus (SCN), which is the master clock in the body [3]. Potentially, the SCN can synchronize clock gene oscillations in all structures related to the control of micturition.

During jet lag, the SCN temporarily loses the ability to generate rhythms and to synchronize body clocks, and it takes about a week for the rhythms to recover [23]. During the adjustment period, the SCN will gradually phase shift while recovering its

rhythm-integration ability. This is reflected at the behavioral level, progressively shifting to the new environmental cycles. Together with these rhythms in locomotor activity, micturition rhythms will also phase shift gradually.

During these processes, timing of urine production will be affected by the shift of drinking behavior. In addition, primitive urine production and water reabsorption in the kidneys [17], which play important role for regulating circadian urine production, may also be affected by jet lag. The urinary bladder also shows diurnal change of capacity to hold urine [9]. Our laboratory previously demonstrated that clock genes in bladder smooth muscle cells play a very important role in the formation of micturition rhythms by regulating the transcription of the gap junction protein Connexin 43 (Cx43), rising in the active phase (night time in the mouse) together with an increase of gap-mediated signals in smooth muscle cells [7]. As Cx43 is only weakly expressed in the resting phase (inactive phase: day time in mice), cholinergic effects are suppressed, and bladder capacity is enlarged [7]. The role of Cx43 in bladder smooth muscle in jet lag-induced micturition changes is a potential route for further investigations.

Here, I found that the time taken to adapt to the new LD cycle in the micturition rhythms is similar to that of locomotor activity rhythms. Since it is speculated that adaptation of the locomotor activity to the new LD cycle is regulated by the SCN [26], similar regulatory mechanism of micturition rhythm should be tested in future studies.

In both micturition and locomotor activity, *Per*-null mice entrained more promptly to the new LD cycles than WT mice under experimental jet-lag conditions. *Per*-null mice

did not show circadian rhythms in constant dark condition [2] since these mice lack the ability to produce endogenous rhythms. Taken together, it seems likely that jet lag symptoms on locomotor activity and micturition are caused due to the stability of the endogenous clock, and paradoxically, an impaired circadian clock may be desirable to alleviate jet lag symptoms.

Clinically, circadian clock may play an important role for maintaining day and night micturition cycle in healthy persons. The present study indicates that micturition cycles are disturbed by jet lag, and it takes 1 to 2 weeks for complete recovery. This point has not been addressed in scientific literature, but may be worth considering since dysregulated and irregular micturition may be a factor contributing to poor sleep in frequent flyers and shift workers.

Reference

1. Cermakian N, Monaco L, Pando MP, Dierich A and Sassone-Corsi P (2001) Altered behavioral rhythms and clock gene expression in mice with a targeted mutation in the Period1 gene. Embo j 20, 3967–3974.

2. Chao HW, Doi M, Fustin JM, Chen H, Murase K, Maeda Y, Hayashi H, Tanaka R, Sugawa M, Mizukuchi N, Yamaguchi Y, Yasunaga J, Matsuoka M, Sakai M, Matsumoto M, Hamada S and Okamura H (2017) Circadian clock regulates hepatic polyploidy by modulating Mkp1-Erk1/2 signalling pathway. Nat Commun 8, 2238.

3. Comperatore CA and Krueger GP (1990) Circadian rhythm desynchronosis, jet lag, shift lag, and coping strategies. Occup Med 5, 323–341.

4. Dibner C, Schibler U and Albrecht U (2010) The mammalian circadian timing system: organization and coordination of central and peripheral clocks. Annu Rev Physiol 72, 517–549.

5. Dunlap JC (1999) Molecular bases for circadian clocks. Cell 96, 271–290.

6. Kiessling S, Eichele G and Oster H (2010) Adrenal glucocorticoids have a key role in circadian resynchronization in a mouse model of jet lag. J Clin Invest 120,

2600–2609.

7. Nakamura S, Kobayashi Y, Tozuka K, Tokue A, Kimura A and Hamada C (1996) Circadian changes in urine volume and frequency in elderly men. J Urol 156, 1275–1279.

8. Negoro H, Kanematsu A, Doi M, Suadicani SO, Matsuo M, Imamura M, Okinami T, Nishikawa N, Oura T, Matsui S, Seo K, Tainaka M, Urabe S, Kiyokage E, Todo T, Okamura H, Tabata Y and Ogawa O (2012) Involvement of urinary bladder Connexin43 and the circadian clock in coordination of diurnal micturition rhythm. Nat Commun 3, 809.

9. Negoro H, Kanematsu A, Matsuo M, Okamura H, Tabata Y and Ogawa O (2013) Development of diurnal micturition pattern in mice after weaning. J Urol 189, 740–746.

10. Okamura H (2004) Clock genes in cell clocks: roles, actions, and mysteries. J Biol Rhythms 19, 388–399.

11. Okamura H, Yamaguchi S and Yagita K (2002) Molecular machinery of the circadian clock in mammals. Cell Tissue Res 309, 47–56.

12. Reddy AB, Field MD, Maywood ES and Hastings MH (2002) Differential resynchronisation of circadian clock gene expression within the suprachiasmatic

nuclei of mice subjected to experimental jet lag. J Neurosci 22, 7326–7330.

13. Reppert SM and Weaver DR (2002) Coordination of circadian timing in mammals. Nature 418, 935–941.

14. Sack RL (2009) The pathophysiology of jet lag. Travel Med Infect Dis 7, 102–110.

15. Schibler U and Sassone-Corsi P (2002) A web of circadian pacemakers. Cell 111, 919–922.

16. Shearman LP, Jin X, Lee C, Reppert SM and Weaver DR (2000) Targeted disruption of the mPer3 gene: subtle effects on circadian clock function. Mol Cell Biol 20, 6269–6275.

17. Stow LR and Gumz ML (2011) The circadian clock in the kidney. J Am Soc Nephrol 22, 598–604.

18. Sugino Y, Kanematsu A, Hayashi Y, Haga H, Yoshimura N, Yoshimura K and Ogawa O (2008) Voided stain on paper method for analysis of mouse urination. Neurourol Urodyn 27, 548–552.

19. Takahashi JS, Hong HK, Ko CH and McDearmon EL (2008) The genetics of mammalian circadian order and disorder: implications for physiology and disease. Nat Rev Genet 9, 764–775.

20. Van Hoeck K, Bael A, Lax H, Hirche H, Van Dessel E, Van Renthergem D and van Gool JD (2007) Urine output rate and maximum volume voided in school-age children with and without nocturnal enuresis. J Pediatr 151, 575–580.

21. Van Hoeck K, Bael A, Lax H, Hirche H and van Gool JD (2007) Circadian variation of voided volume in normal school-age children. Eur J Pediatr 166, 579–584.

22. Weiss JP, Blaivas JG, Stember DS and Chaikin DC (1999) Evaluation of the etiology of nocturia in men: the nocturia and nocturnal bladder capacity indices. Neurourol Urodyn 18, 559–565.

23. Witjes WP, Wijkstra H, Debruyne FM and de la Rosette JJ (1997) Quantitative assessment of uroflow: is there a circadian rhythm? Urology 50, 221–228.

24. Wood R, Eichel L, Messing EM and Schwarz E (2001) Automated noninvasive measurement of cyclophosphamide-induced changes in murine voiding frequency and volume. J Urol 165, 653–659.

25. Yagita K, Tamanini F, van Der Horst GT and Okamura H (2001) Molecular mechanisms of the biological clock in cultured fibroblasts. Science 292, 278–281.

26. Yamaguchi Y, Suzuki T, Mizoro Y, Kori H, Okada K, Chen Y, Fustin JM, Yamazaki F, Mizuguchi N, Zhang J, Dong X, Tsujimoto G, Okuno Y, Doi M and Okamura H (2013) Mice genetically deficient in vasopressin V1a and V1b receptors are

resistant to jet lag. Science 342, 85–90.

27. Yoshimura N and Chancellor MB, Physiology and Pharmacology of the Bladder. Abdominal Key at https://abdominalkey. com/physiology-and-pharmacology-of-the-bladder-and-urethra/

28. Yoshimura N and de Groat WC (1997) Neural control of the lower urinary tract. Int J Urol 4, 111–125.

29. Zheng B, Larkin DW, Albrecht U, Sun ZS, Sage M, Eichele G, Lee CC and Bradley A (1999) The mPer2 gene encodes a functional component of the mammalian circadian clock. Nature 400, 169–173.

Acknowledgement

First of all, I wish to express sincere thanks to Prof. Hitoshi Okamura, Dr. Fustin Jean-Michel, Prof. Masao Doi, Dr. Chao Hsu-Wen for their direction and kind encouragement throughout my graduated study.

I would like to thank Dr. Masahito Ikawa and Asami Oji from Osaka University for their kind support in producing mutant mice.

I am grateful to all the members of Okamura lab Fustin lab, and Doi lab members for their advice and help.

I thank my parents and wife for their support and encouragement. Without their support, I would not have accomplished this thesis.

I would like to thank to Japan Society for the Promotion of Science for Young Scientists for financial support during my doctoral course.